Covalent Conjugation of Small Molecule Inhibitors and Growth Factors to a Silk Fibroin-Derived Bioink to Develop Phenotypically Stable 3D Bioprinted Cartilage

Nilotpal Majumder, Chandrashish Roy, Laura Doenges, Ivan Martin, Andrea Barbero, and Sourabh Ghosh*

Cite This: https://doi.org/10.1021/acsami.3c18903

Read Online

ACCESS | Metrics & More | Article Recommendations | Supporting Information

ABSTRACT: Implantation of a phenotypically stable cartilage graft could represent a viable approach for repairing osteoarthritic (OA) cartilage lesions. In the present study, we investigated the effects of modulating the bone morphogenetic protein (BMP), transforming growth factor beta (TGFβ), and interleukin-1 (IL-1) signaling cascades in human bone marrow stromal cell (hBMSC)-encapsulated silk fibroin gelatin (SF-G) bioink. The selected small molecules LDN193189, TGFβ3, and IL1 receptor antagonist (IL1Ra) are covalently conjugated to SF-G biomaterial to ensure sustained release, increased bioavailability, and printability, confirmed by ATR-FTIR, release kinetics, and rheological analyses. The 3D bioprinted constructs with chondrogenically differentiated hBMSCs were incubated in an OA-inducing medium for 14 days and assessed through a detailed qPCR, immunofluorescence, and biochemical analyses. Despite substantial heterogeneity in the observations among the donors, the IL1Ra molecule illustrated the maximum efficiency in enhancing the expression of articular cartilage components, reducing the expression of hypertrophic markers (re-validated by the GeneMANIA tool), as well as reducing the production of inflammatory molecules by the hBMSCs. Therefore, this study demonstrated a novel strategy to develop a chemically decorated, printable and biomimetic SF-G bioink to produce hyaline cartilage grafts resistant to acquiring OA traits that can be used for the treatment of degenerated cartilage lesions.

KEYWORDS: osteoarthritis, signaling pathway, chondrogenesis, silk fibroin gelatin bioink, 3D bioprinting, chondrocyte hypertrophy
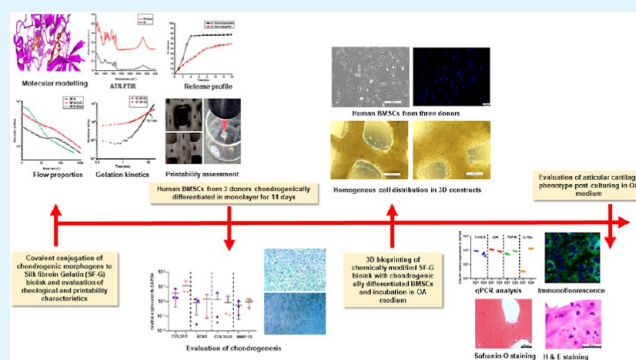
1. INTRODUCTION

The progressive degeneration of articular cartilage tissue is a significant hallmark during osteoarthritis (OA) advancement.[1] The surrounding inflammatory microenvironment of the joint tissue following the onset of OA alters the articular chondrocytes, both phenotypically and genotypically marked by cell-clustering,[2,3] production of mechanically inferior collagen matrices, and proteoglycan loss.[4] The increase in cell volume,[5] matrix calcification, and vascular ingrowth allows for the conversion of the native hyaline healthy state to an aberrant hypertrophic phenotype through a process termed "hypertrophic differentiation".[6] The alteration in the healthy articular chondrocytes in the adult joint is similar to the natural "endochondral ossification process", regulating the longitudinal growth of the long bones. This is characterized by an increase in the cell proliferation rate and expression of hypertrophic markers like collagen type-X (COL10A1, COL-X), RUNX family transcription factor 2 (RUNX2), and alkaline phosphatase and osteopontin (OPN). This led cartilage biologists to incorporate principles from developmental

biology, material science, and cell biology to synthesize an advanced cartilage tissue graft as a plausible regenerative therapy for OA.[7]

Despite several unprecedented efforts in cartilage tissue engineering for nearly 4 decades, fabricating a phenotypically stable articular cartilage graft remains a significant roadblock. Researchers around the globe have utilized the combination of several advanced biomaterials and cell types like chitosan—hyaluronic acid with articular chondrocytes,[8] alginate—gellan gum with murine bone marrow-derived mesenchymal stem/stromal cells (BMSCs),[9] or poly(vinyl alcohol)-gelatin hydrogels with human BMSCs (hBMSc)[10] to fabricate articular cartilage tissue grafts with adequate mechanical, viscoelastic,

A

and biological characteristics. Scientists have also deployed different scaffolding techniques like electrospinning with polycaprolactone−gelatin composite[10] to freeze−drying using silk−chitosan blend[11] for applications spanning from injectable biphasic hydrogels[12] to growth factor-loaded acellular implantable cartilage grafts.[13] Our laboratory has also been instrumental in augmenting the technological supremacy of 3D bioprinting and pro-chondrogenic ascendancy of silk fibroin gelatin (SF-G) biomaterial to fabricate neo-cartilage tissue grafts with murine BMSCs[14] and human articular chondrocytes.[15] The 3D bioprinted constructs demonstrated long-term cell viability and activation of the pro-chondrogenic Wnt/β-catenin signaling cascade.[16] There are also reports of successful chondrogenesis poststimulation of BMSCs with an array of growth factors like transforming growth factor-β (TGFβ),[14,17] bone morphogenetic protein (BMP),[18,19] platelet-derived growth factor (PDGF),[20] and insulin-like growth factor (IGF)[21] owing to their high proliferation ability, ease of availability, and the ability to be differentiated into multiple tissue types.[22,23] Moreover, the majority of the research works focused on hyaline cartilage formation in vitro under normal chondrogenic culture conditions rather than evaluating the maintenance of stable articular cartilage phenotype in vitro under OA-mimicking microenvironment. As a result, a hypertrophic phenotypic drift occurs in the implanted cartilage grafts.[24]

However, the major drawback of using BMSC, even from adult tissues, for the engineering of therapeutic cartilage grafts lies in the fact that these cells are intrinsically committed toward terminal hypertrophic differentiation upon induction of chondrogenesis and subsequent bone formation of this cartilaginous template via the endochondral program.[25] Moreover, supplements (insulin,[26] ascorbic acid,[27] TGFβ,[28] and BMP[29]) provided during the chondrogenic differentiation protocol have been reported to induce chondrocyte hypertrophy through the activation of osteogenic and dysregulated functioning of chondrogenic signaling cascades. This led the progressive group of tissue engineers to delve deep into the intricate molecular mechanisms governing the activation and inhibition of respective cellular signaling events to promote chondrogenesis while simultaneously hindering hypertrophy.[30,31]

In that regard, Chawla et al. have endorsed the role of the BMP signaling pathway in OA development by exogenous treatment of the microcartilage model. When the OA microcartilage model was primed with BMP cascade small molecule inhibitor, low dose naltrexone (LDN193189), a reduction in chondrocyte hypertrophy markers such as Matrix metalloproteinase-1/13 (MMP-1/13) and COL-X with an upregulation of BMP antagonist Gremlin (GREM1) was observed.[32] The selectivity of LDN193189 toward inhibition of the OA-inducing BMP signaling pathway has been well ascribed by Cannon et al.[33] and Boergermann et al.[34] The presence of an inflammatory microenvironment and its contribution to articular cartilage degeneration through the activation of the interleukin-1β (IL-1β) pathway is well established.[35,36] As a consequence, research groups have proposed the use of interleukin 1 receptor antagonist (IL1Ra)[37] in the directly injectable form[38] or in polylactic-co-glycolic acid (PLGA) microspheres[39] to competitively bind to the IL-1 receptor and promote cartilage healing through its anti-inflammatory effect. Furthermore, the chondro-stimulatory role of the TGFβ signaling cascade through the small

mother against decapentaplegic (SMAD 2/3) route in different stages of embryonic cartilage development has been extensively elucidated by van der Kraan et al.[16,28] This led researchers to utilize TGFβ in chondrogenic differentiation media either in the exogenous form[16,40] or immobilized into a polymer-based delivery system[41] to ensure maximum exposure to the cultured cells. However, the major challenge lies in the shorter half-life of the respective small molecules (LDN193189: 1.6−4 h,[42] IL1Ra: 4−6 h[43]) and pro-chondrogenic cytokine TGFβ3 (50 min).[44] This causes rapid clearance if injected directly in vivo or requires frequent replenishment when exogenously added to the media, limiting its bioavailability.

Therefore, in this work, we intend to examine the pro-chondrogenic and antihypertrophic properties of our chosen small molecules and growth factors (LDN193189, IL-1Ra, and TGFβ3) chemically/covalently conjugated to our proprietary SF-G biomaterial and 3D bioprinted using chondrogenically differentiated human bone marrow stromal cells (hBMSCs). The primary objective of this research lies in investigating whether tuning the cell signaling pathways (BMP, TGFβ, and IL-1β) permits the BMSC-derived chondrocytes within the chemically decorated SF-G constructs to retain the hyaline chondrocyte phenotype when cultured in an "OA-inducing medium". In particular, we first tested the feasibility of covalently conjugating LDN193189, IL-1Ra, and TGFβ3 to the SF-G biomaterial without affecting the rheological and printability characteristics. We then used the modified SF-G bioink to generate 3D bioprinted hBMSC-based cartilage constructs. The SF-G constructs have already shown around 86% cell viability when cultured until day 30. We also investigated the effect of the conjugated molecules in modulating the responses of chondrogenic differentiated hBMSCs once exposed to hypertrophy-enhancing factors[24] as well as to a low-grade inflammatory cytokine cocktail containing IL1β, interleukin 6 (IL6), and tumor necrotic factor α (TNFα) to mimic inflamed synovial fluid.[45]

2. MATERIALS AND METHODS

2.1. Computational Modeling of Bioconjugation. The structure-based virtual screening process involved obtaining the ligand structures (LDN193189, TGFβ3, and IL-1Ra) from PubChem and Protein Data Bank. The protein structures were prepared for docking using UCSF Chimera software by removing the nonstrand residues, while the ligand analysis was conducted using UCSF Chimera, followed by Autodock Vina docking. A blind docking procedure was performed, and the docked structures were analyzed to identify the one with the lowest c-score, indicating the most favorable binding energy. To assess hydrophobic interactions and calculate the root-mean-square deviation (RMSD) value, PyMol software was used, ensuring the accuracy and quality of the final docked structure. The Ramachandran plot of the respective small molecule conjugated SF was plotted using UCSF Chimera to assess the favorable regions of amino acid residues, which were further verified using Discovery Studio Visualizer software. Our rigorous computational approach, incorporating tools such as UCSF Chimera, Autodock Vina, and PyMol, ensured the accuracy of these results.

2.2. Preparation of SF Solution. The SF solution was prepared using a combination of three methods: degumming, dissolution, and dialysis, as described previously.[46,47] The silk cocoons procured from Central Silk Board (Bangalore, India) were diced into fine pieces before they were boiled in 0.02 M sodium carbonate (Na$_2$CO$_3$, Fisher Scientific) solution for 20 min to remove the sericin component. The SF fibers were washed in deionized water multiple times to remove residual sericin and dried at 37 °C overnight in the oven. The dissolution was done to get pure silk solution by dissolving the dried

silk fibers in a 9.3 M lithium bromide (LiBr, SRL) solution and incubating at 60 °C for 4 h. The concentration of the silk solution was evaluated (5%) and autoclaved for further experiments.

2.3. Chemical Modification of SF Biomaterial. *2.3.1. Cyanuric Chloride-Mediated Coupling of LDN193189 and TGFβ3.* For chemical cross-linking of LDN193189 and TGFβ3 with SF-G biomaterial, the protocol devised by Gotoh et al. was followed with slight modifications.[48] The binder solution used was cyanuric chloride (CyCl) deployed at an effective concentration of 30% (previously optimized, data not shown). The 30% CyCl solution (Sigma-Aldrich) was prepared by dissolving the CyCl powder in 1 mL of the 1,4-dioxane solution, followed by rigorous mixing. The prepared 5% silk solution (5SF) was mixed with sodium bicarbonate (NaHCO$_3$) and CyCl solution in a ratio of 1:3:1. The reaction was carried out at 4 °C for 1.5 h. The CyCl-modified 5SF solution was further mixed with the respective small molecule (LDN193189, 50 nM, Sigma-Aldrich[32]) and growth factor (TGFβ3, 10 ng/mL, ProSpec[16]) to prepare the final conjugated solution.

2.3.2. Diazonium Coupling-Mediated Cross-Linking of IL-1Ra. The diazonium stock solution was prepared by mixing 1.6 M p-toluene sulfonic acid and 0.8 M sodium nitrite. To this, 5SF silk solution prepared in borate buffer was added to prepare a 1 mL diazonium coupled silk solution. The IL-1Ra (ProSpec) at a concentration of 500 ng/mL[49] was added to the diazotized SF solution and diluted 1000-fold, allowing for the reaction for 2 h.[50]

2.4. Physiochemical Characterization. *2.4.1. Attenuated Total Reflectance Fourier Transform Infrared Spectroscopy.* The FTIR measurements were taken in ATR mode for all the test samples using a PerkinElmer ATR-FTIR spectrometer (Spectrum BX Series, MA, USA) scanned with a resolution of 4 cm^{-1} for up to 50 scans.[51] The Fourier self-deconvolution (FSD) spectra were generated using OriginPro 2021 (OriginLab Corporation, Northampton, MA, USA). The conjugation of SF and CyCl was confirmed via C−O−C stretching between 1050 and 1250 cm^{-1}. Any unreacted CyCl will appear as peaks in the 600−800 cm^{-1} range. The diazotization of 5SF solution was examined from the respective peaks in the range of 700−800 and 1000−1200 cm^{-1}, respectively. The FSD spectra were fitted with Gaussian profiles to estimate the secondary conformation change in the amide-I region (1595−1705 cm^{-1}). The region between 1616 and 1637 and 1695−1705 cm^{-1} corresponded to the β-sheet content, which was calculated by integrating the area under the respective region bands compared to the total amide-I bands.

2.4.2. UV−Visible Spectroscopy. The chemical validation of diazotization of SF biomaterial was further confirmed by spectroscopically measuring the concentration of azo incorporation at the tyrosine residues of SF measured at a λ_{max} of 274 nm using a UV−visible spectrophotometer (Thermo Scientific).

2.4.3. In vitro Release Kinetics of LDN19389, TGFβ3, and IL1Ra. The release profile of the respective small molecules and growth factor was evaluated by immersing the chemically decorated SF matrices in simulated body fluid (SBF) at 37 °C for 14 days under constant shaking.[52] The SBF was buffered at pH 7.4 using a 75 mM Tris Buffer. Samples were retrieved at regular intervals and were replaced with equal volumes of SBF. The release kinetics of LDN193189 were calculated using UV−visible spectroscopy, whereas TGFβ3 and IL-1Ra were examined using their respective ELISA kits (Make-FineTest) following the manufacturer's protocol.

2.5. Preparation of SF-G Bioink. To prepare a bioink comprising of 5% SF solution and 6% gelatin (SF-G),[9,53] an appropriate quantity of ethanol sterilized gelatin was weighed (60 mg for 1 mL bioink), and to it, 10% fetal bovine serum (FBS, Gibco) and 10% minimum essential medium (MEM, Himedia) were added. The remaining volume makeup was carried out by adding 5% silk solution and further allowed to form a clear composite solution at 37 °C. The SF-G blend was further enzymatically cross-linked, adding 800 U of mushroom tyrosinase (Sigma-Aldrich) enzyme.

2.6. Rheological Analysis. The effect of chemical modification of the SF biomaterial with cyanuric chloride and diazonium coupling on the rheological properties of the SF-G bioink was analyzed by investigating the viscosity and gelation profiles of the conjugated SF-G

bioinks.[46,54] The flow behavior of the respective chemically modified SF-G bioinks was calculated by evaluating their viscosity profiles against an increasing shear rate from 1 to 1000 s^{-1}. All the measurements were carried out in an Anton Parr MCR302 plate and plate Rheometer at 25 °C. The gelation kinetics of all the chemically modified bioinks were examined using Time sweep analysis with 1% strain and 1 Hz frequency.

2.7. Printability Analysis. To evaluate whether the chemical modifications affected the printability characteristics, the acellular SF-G bioink was 3D bioprinted using a direct write assembly (Fiber Align, Aerotech Inc., USA) at 25 °C and 22 PSI pressure up to 4 layers. The mushroom tyrosinase-cross-linked chemically modified SF-G bioinks were deposited using a 210 µm nozzle at a speed of 1 mm/s. The printability was measured as a function of the pore dimension, which is given as

$$P = L^2/16A$$

L and A represent the perimeter and the area of the respective pores, respectively, which are measured using ImageJ software from the microscopic images of the constructs.[9] The spreading ratio was calculated as the ratio of the diameter of the extrudate to the diameter of the printer nozzle.[46]

2.8. Expansion and Chondrogenic Differentiation of Human Bone Marrow-Derived Mesenchymal Stem Cells. The hBMSCs were isolated from the bone marrow samples obtained from three different donors (donor-1: female, 43 years, donor-2: male, 18 years, donor-3: female, 28 years) after obtaining informed consent during orthopedic surgical procedures in accordance with the local ethical committee (University Hospital Basel; Prof. Dr. Kummer; approval date 26/03/2007 ref number 78/07). Cells were expanded until passage 2 in MEM-α (α-MEM, Gibco) supplemented with 1% antibiotic−antimycotic solution (Gibco), 10% FBS (Gibco), and 5 ng/mL FGF-2 (Prospec). Expanded hBMSCs were frozen in FBS containing 10% dimethyl-sulfoxide (DMSO, Himedia) and shipped from Basel to Prof S. Ghosh's laboratory, where they were expanded for an additional passage before their chondrogenic culture. The chondrogenic medium comprised of Dulbecco's modified eagles medium/nutrient mixture F-12 (DMEM/F-12, Gibco) supplemented with 1% human serum albumin (HSA, Sigma-Aldrich), 1% sodium pyruvate (Gibco), 1% HEPES (Gibco), 1% antibiotic−antimycotic solution (Gibco), 1% insulin-transferrin-selenium (ITS) + premix (Gibco), 10 ng/mL TGFβ3 (Prospec Biosystems), 10^{-7} M dexamethasone (Sigma-Aldrich), and 0.1 mM ascorbic acid 2-phosphate (Sigma-Aldrich) for 14 days. The media was changed twice every week.

2.9. Evaluation of Chondrogenesis of hBMSCs. The extent of chondrogenesis of hBMSCs after 14 days of monolayer culture in chondrogenic (vs expansion medium) was analyzed by qPCR or histologically (Alcian blue staining). The RNA from the monolayer culture on day 14 was extracted, and the cDNA from the isolated RNA was reverse-transcribed, followed by qPCR using a SYBR Green Master Mix (as described in session 2.12). The genes evaluated are COL2A1, SOX9, COL10A1, and MMP-13.[18,55] Alcian blue staining was performed to evaluate the GAG deposition after 14 days of chondrogenic differentiation of hBMSCs. A 1% Alcian blue stain was mixed with 3% aqueous acetic acid to perform the staining at an acidic pH of 2.5.

2.10. 3D Bioprinting of Cell Encapsulated Chemically Modified SF-G Bioink. The chondrogenically differentiated hBMSCs at a density of 1 million cells/mL were encapsulated in the chemically decorated SF-G biomaterial. The cell-laden bioink was loaded into a sterile barrel capped with a nozzle of 250 µm diameter and fitted to a 3-axis robotic framework of the direct write assembly system (Fiber Align, Aerotech Inc., USA). The 6-layered 6 mm × 6 mm 3D CAD model was developed using RoboCAD software. The printing was carried out at a temperature of 25 °C with a speed of 1 mm/s and 22 ± 4 PSI pressure. Postprinting, the 3D bioprinted constructs were allowed to gain structural stability through enzymatic cross-linking of mushroom tyrosinase for 20 min. The cross-linked 3D constructs with chondrogenic hBMSCs were incubated in hyper-

Table 1. List of Analyzed Genes Using RT PCR

gene	full name	gene globe ID	catalog no.
GAPDH	glyceraldehyde-3-phosphate-dehydrogenase	PPH00150F-200	330001
COL2A1	collagen type II alpha 1 chain	PPH02134F-200	330001
SOX9	SRY-box transcription factor 9	PPH02125A-200	330001
COL10A1	collagen type X alpha 1 chain	PPH02120E-200	330001
MMP-13	matrix metalloproteinase 13	PPH00121B-200	330001
SMAD-4	suppressor of Mothers against Decapentaplegic 4	PPH00134C-200	330001
PRG-4	proteoglycan 4	PPH06096E-200	330001
NOG	noggin	PPH01926A-200	330001
DKK1	Dickkopf 1	PPH01752C-200	330001
TGFβR1	transforming growth factor beta receptor 1	PPH00237C-200	330001

trophic differentiation media with inflammatory conditions, which will be now termed an "OA-inducing medium". Here, an "OA-inducing medium" comprised of DMEM/F-12 medium added with 1% HSA (Sigma-Aldrich), 1% sodium pyruvate (Gibco), 1% HEPES (Gibco), 1% antibiotic−antimycotic (Gibco), 1% insulin-transferrin-selenium (ITS) + premix (Gibco), 0.1 mM ascorbic acid 2-phosphate (Sigma-Aldrich), 10^{-7} M dexamethasone (Sigma-Aldrich), 0.01 M β-glycerophosphate (Sigma-Aldrich), and 50 nM L-thyroxine (Sigma-Aldrich) additionally supplemented with 0.05 ng/mL IL-1β, 0.05 ng/mL TNFα, and 0.1 ng/mL IL-6.[45]

2.11. Histological Analysis. The 3D bioprinted constructs from the respective groups at day 28 (day 14 + 14) were harvested, washed with PBS, and fixed with 4% paraformaldehyde for 20 min, followed by dehydration at gradient alcohol concentrations.[9] The sGAG deposition was analyzed using Safranin O staining and Alcian Blue staining, whereas the cellular morphology was evaluated using Haematoxylin and Eosin Staining.

2.12. Gene Expression Analysis. The 3D bioprinted constructs from the respective groups (SF-G, SF-G-LDN, SF-G-TGFβ, and SF-G-IL1Ra) of each donor were digested using 250 μg/mL Protease XIV (Sigma) solution for 20 min at 37 °C to isolate the encapsulated cells.[56] The cell lysates from all the sample groups were collected at two different time points postincubation in a hypertrophic differentiation medium: day 21 (day 14 + 7) and day 28 (14 + 14). The total RNA was isolated from the respective samples using an RNeasy kit column (Qiagen) per the manufacturer's protocol. The corresponding cDNA was isolated using a first-strand cDNA synthesis kit (Qiagen). The qPCR was carried out using a SYBR Green Master Mix (Qiagen) in a Rotor-Gene Q Thermocycler (Qiagen). The primers used for the analysis were COL2A1, SOX9, COL10A1, MMP-13, SMAD-4, PRG-4, NOG, DKK1, TGFβR1, and GAPDH, which was considered the housekeeping gene, whereas monolayer day 1 culture was used for normalization. All the experiments were carried out in triplicates (n = 3). The list of analyzed genes is mentioned in Table 1.

2.13. Protein Expression Analysis. The protein expression analysis was carried out using immunofluorescence studies. Briefly, the 3D bioprinted constructs of donor-2 hBMSCs at day 28 (day 14 + 14) from the respective groups were fixed with BD Cytofix/Cytoperm solution (BD Biosciences) for 20 min, followed by washing twice with BD Perm/Wash buffer. The blocking was carried out by incubating the individual constructs with 8% BSA (Thermo Scientific) solution for 1 h at room temperature. Subsequently, the constructs were incubated with mouse anticollagen II (5 μg/mL, DSHB) and mouse anticollagen X (5 μg/mL, DSHB) primary antibodies prepared in 2% BSA solution overnight. The constructs were washed twice with PBS, followed by incubation with anti-mouse Alexa Fluor 488 (2 μg/mL, Thermo Fisher Scientific) for 2 h and rinsed with PBS solution twice. The samples were then stained with DAPI (1 μg/mL, Thermo Fisher Scientific) for 15 min, rewashed with PBS twice to remove the excess stain, and visualized under a Leica SP5 inverted confocal laser scanning microscope (Leica Systems).

2.14. Biochemical Analyses. The amounts of different by-products released during cell metabolism during the chondrogenic culture of the hBMSCs were quantified. The supernatants at day 28

(14 + 14) were collected from each sample group cultured under different conditions. The nitrite content, total lipid peroxidation and total nitric oxide (TNO) release profile of the chondrogenically differentiated hBMSCs within the SF-G constructs when cultured in a hypertrophic medium was evaluated using an EZ Assay TBARS assay kit and EZ Assay Nitric Oxide assay kit as per the manufacturer's protocol.[51,57] The amount of glycosaminoglycans (GAG) deposited in the constructs post 14 days of hypertrophic differentiation was quantified using a Dimethyl methylene blue (DMMB) assay. Briefly, the cationic dye DMMB interacts with the negatively charged GAG (sGAGs), followed by a color change spectrophotometrically measurable at 525 nm with chondroitin sulfate as standard. All experiments were performed in triplicates (n = 3).

2.15. Gene Analysis Using GeneMANIA. GeneMANIA software was used to predict the correlation and interaction of the input genes with the pool of genes associated with articular cartilage homeostasis. Through this analysis, we can validate the importance of the chosen set of genes for qPCR.[58] Furthermore, all the experimental groups were chosen from one single donor showing maximum chondrogenic characteristics (donor-2) and the respective 5 upregulated genes of each experimental group were selected for the analysis. The different colors represent the different forms of interactions between the respective genes.

2.16. Statistical Analysis. The statistical analysis was performed using GraphPad Prism 7 software (San Diego, California, USA). One-way ANOVA, followed by Bonferroni's multiple comparison tests, was performed to demonstrate the statistical significance between various groups, whereas an unpaired t-test was used to compare two individual groups. All the experiments were carried out in technical triplicates with the mean values represented with ±standard deviation with $p < 0.05$ as the statistical significance value.

The similarity between the respective donors (donor-1, donor-2, and donor-3) was carried out by evaluating the Euclidean distance and similarity percentage matrices based on the gene expression values of different experimental groups of each donor. Briefly, for each pair of donors (donor-1 vs donor-2, donor-2 vs donor-3, and donor-3 vs donor-1), the Euclidean distance was calculated between each gene expression value and the maximum distance is evaluated as the sum of Euclidean distances between two donor's gene expression values. Further, the similarity percentage was calculated using the formula: similarity percentage = ((max distance − euclidean distance)/max distance) × 100. The 2D line plot and the corresponding heat map were generated using the Python Jupyter platform.

3. RESULTS

3.1. Computational Prediction of Conjugation of Small Molecules and Growth Factors to the SF Biomaterial. Advanced computational tools were used to examine the binding strengths between various small molecules (ligands) and their respective target protein, namely, SF. The results revealed that SF-CyCl-LDN exhibited the strongest binding affinity with an impressive C-score of −11.54, followed closely by SF-Diazo-IL1Ra with a C-score of −8.5. The SF-
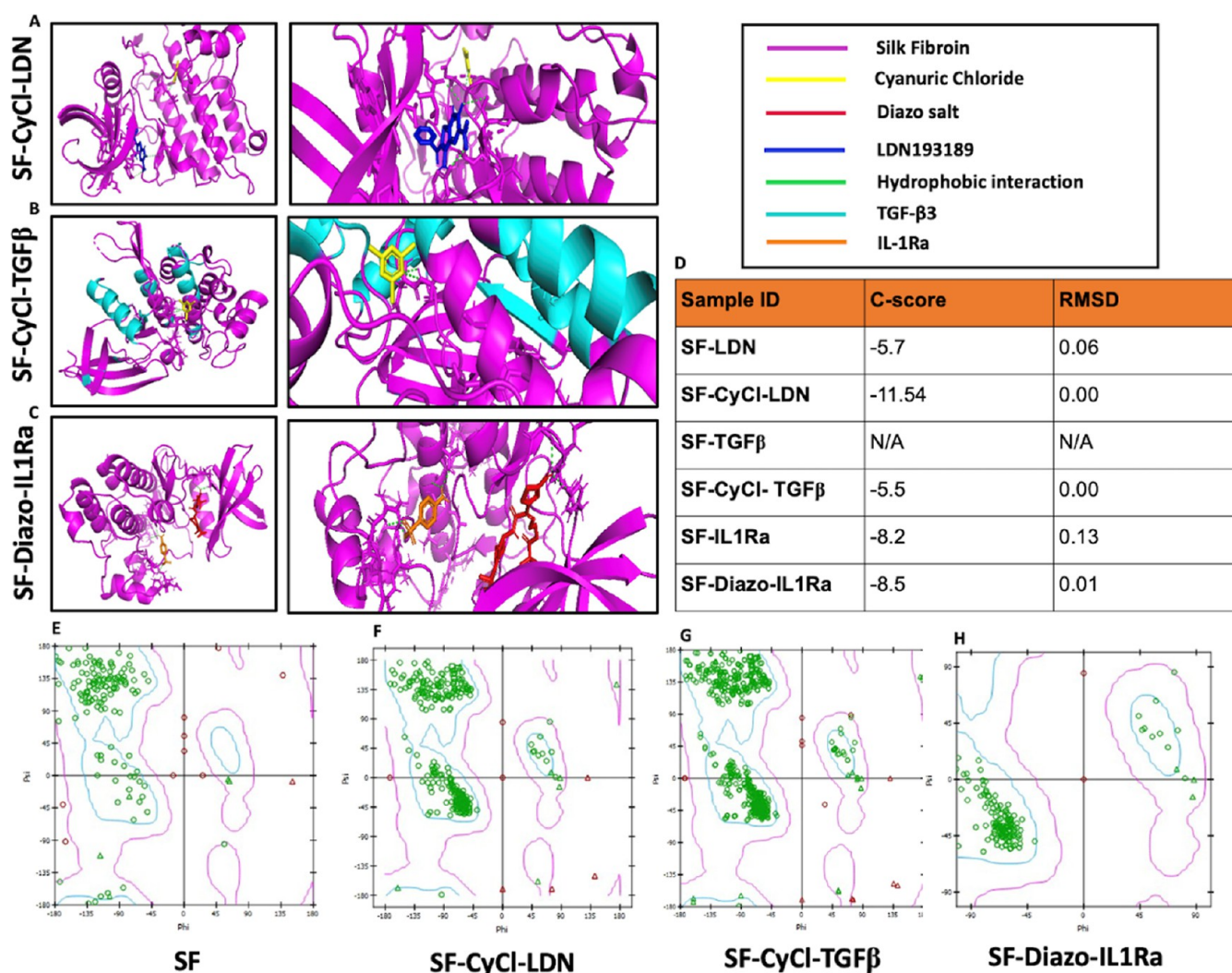
Figure 1. (A−C) Computational modeling prediction of small molecule and growth factor conjugation with the chemically modified SF biomaterial, (D) model with the lowest C-score demonstrated stronger binding affinity and (E−H) Ramachandran plot illustrated the native conformation of the amino acid residues post-chemical modification of the SF biomaterial with cyanuric chloride (CyCl) and diazonium salt (Diazo), respectively.

CyCl-TGFβ displayed a moderate interaction with a C-score of −5.5. The SF-IL1Ra with a C-score of −8.2 and SF-LDN (C-score: −5.7) also showed a moderate binding affinity, while SF-TGFβ demonstrated no discernible interaction (Figure 1A−D). In homology modeling, a lower C-score indicates a better fit of the modeled structure to experimental data and known structural templates. This implies a more accurate representation of the docked protein structure. Lower C-scores correlate with more accurate predictions of binding affinity between interacting proteins. This information can be valuable in understanding the strength and specificity of the interaction.

Additionally, the Ramachandran Plot (Figure 1E−H) demonstrated the structural stability of these small molecule conjugated SF complexes. For SF-CyCl-LDN, the hydrophobic interaction between the glutamic acid 260 (GLU 260) and asparagine 261 (ASN 261) residues, the electrostatic interactions between the charged leucine 357 (LEU 357) and arginine 218 (ARG 218) residues and the cyclic structure of proline 430 (PRO 430) contributed to the structural stability of the complex. Similarly, the hydrophobic interactions between the methionine 288 (MET 288) and phenylalanine 324 (PHE 324) residues, the ionic interactions

between the positively charged arginine 218 (ARG 218) and lysine 346 (LYS 346) amino acid residues, and the hydrogen bond interaction between the polar glutamine 228 (GLN 228) and tyrosine 219 (TYR 219) residues aided in the structural stability of the SF-CyCl-TGFβ complex. Additionally, flexible residues like glycine 229 (GLY 229) and serine 364 (SER 364) allow the complex to adapt to varying thermal conditions without compromising its stability. Furthermore, for SF-Diazo-IL1Ra conjugate, the same hydrophobic interactions (arginine 416 and phenylalanine 324) and electrostatic interactions (lysine 346 and aspartic acid 433) rendered the complex stable. The additional role of cysteine 449 in forming disulfide linkages and valine 450 in showing hydrophobic interactions is also underlined in the Ramachandran plot.

3.2. Experimental Validation of Chemical Modification of SF Biomaterial. *3.2.1. ATR FTIR Characterization.* The cyanuric chloride-based approach was adopted to chemically conjugate the small molecule LDN193189 and TGFβ3 growth factor with the SF biomaterial. The triazine ring of the cyanuric chloride is known to be substituted with the hydroxyl moieties of the tyrosine residues on the one hand and react with the hydroxyl or amino groups on the other hand
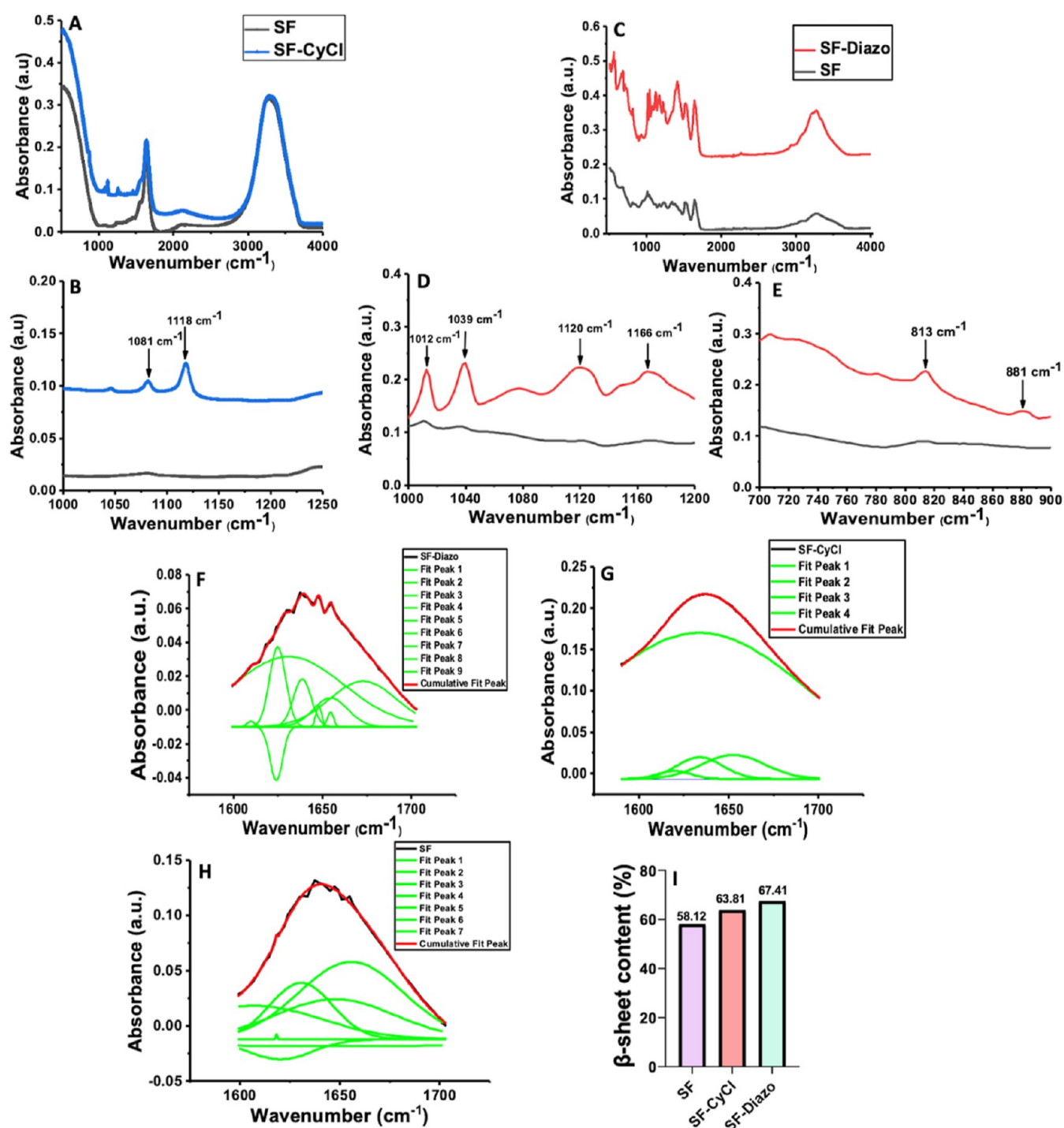
Figure 2. ATR-FTIR characterization, (A,B) cyanuric chloride (CyCl) modification of SF biomaterial demonstrating peak at respective C−O−C bonding region, (C−E) diazonium coupling modification of SF biomaterial showing peaks at respective C−N bonding and S−H stretching regions, (F−H) deconvolution of the amide-I region (1590−1710 cm^{-1}) for the respective SF-CyCl, SF-Diazo, and SF (untreated) group, and (I) quantification of the beta-sheet content from the deconvoluted spectra.

to accentuate its role as a coupling reagent. A medium-intensity peak in the ether bonding region (C−O−C) confirmed the conjugation of CyCl with the SF biomaterial (Figure 2A,B). Further, representative peaks at 781 and 813 cm^{-1} within the S−O stretching region confirmed the diazo incorporation in our SF-G bioink. Additionally, high-intensity peaks at 1012, 1039, 1080, 1120, and 1172 cm^{-1} due to CN bond formation during the diazonium coupling reaction further validated the claim (Figure 2C−E). The secondary

conformation change post CyCl modification of SF was evaluated by deconvoluting the 1600−1700 cm^{-1} region and calculating the β-sheet content. The highest β-sheet content was observed in the SF-Diazo group (67.41%), followed by the SF-CyCl group (63.81%) compared to the control group (58.12%). Thus, chemical modification of SF material enhanced the β-sheet content.

3.2.2. UV Visible Spectroscopy. UV visible spectroscopy was deployed to characterize the azo incorporation into the silk
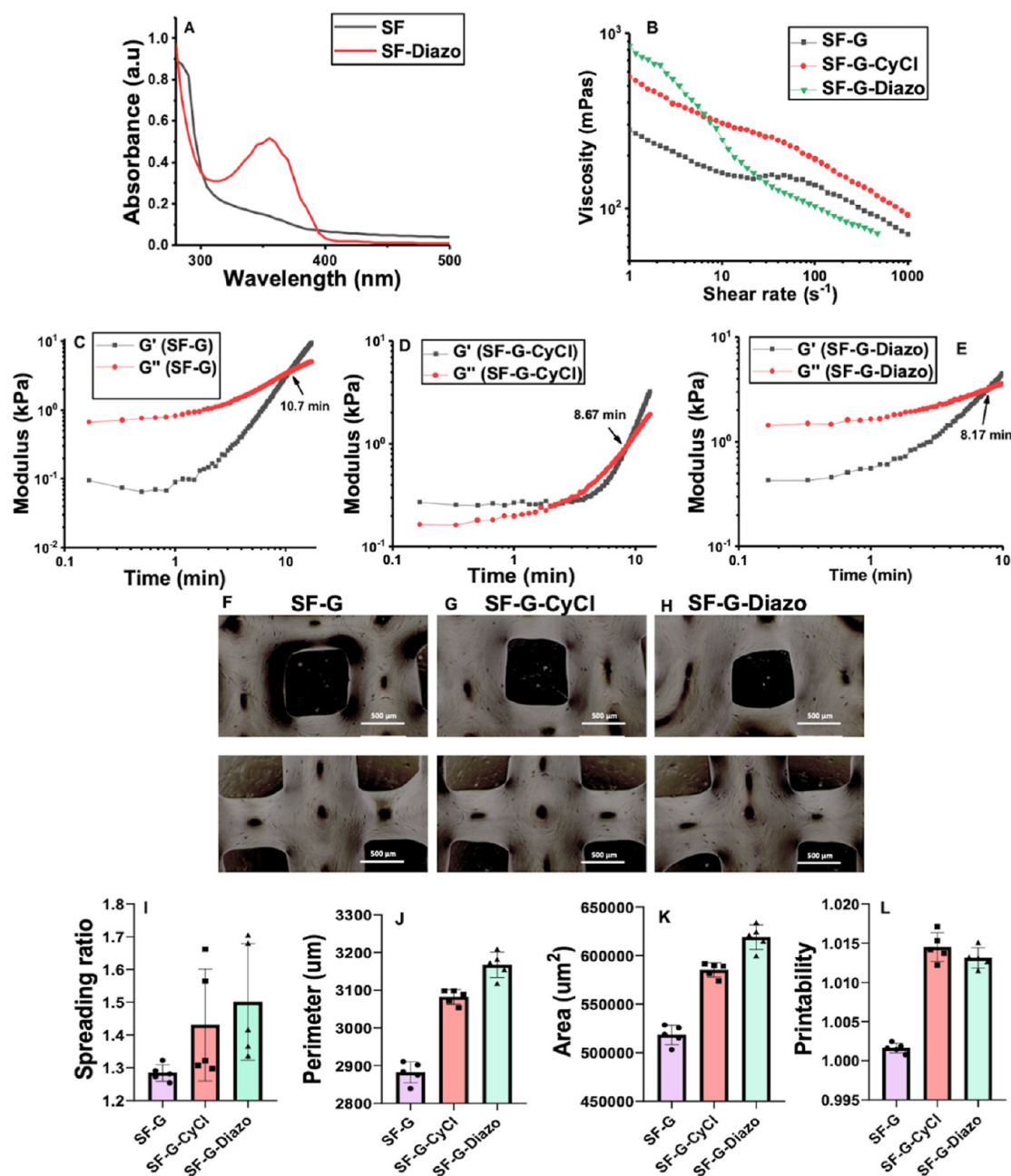
Figure 3. (A) UV visible spectroscopy of azo incorporation by diazonium coupling in SF biomaterial, (B) flow curve of the chemically modified SF-G bioinks showing characteristic shear-thinning behavior of both the chemically decorated bioinks, (C) gelation kinetics of untreated mushroom tyrosinase cross-linked SF-G bioink, (D) gelation kinetics of mushroom tyrosinase cross-linked SF-G-CyCl bioink, (E) gelation kinetics of mushroom tyrosinase cross-linked SF-G-Diazo bioink, (F–H) optical microscopic images of the 3D constructs printed with respect acellular chemically modified SF-G bioinks, (I) quantification of the spreading ratio (n = 5), (J) quantification of the printability index (n = 5), (K) quantification of the perimeter of the pore (n = 5), and (L) quantification of the area of the pore (n = 5). Here, n = 5 corresponds to the evaluation of the respective parameter from 5 different regions.

Table 2. Quantification of % Tyrosine Residues Modification of SF Upon Diazonium Coupling

sample	absorbance (nm)	extinction coefficient (M^{-1} cm^{-1})	azo conc. (mM)	silk conc. (mM)	% tyrosine residues modified
untreated silk	0.05	22,000	0	2.69×10^{-7}	0
diazotized silk	0.525	22,000	2.5×10^{-5}	2.69×10^{-7}	76.9

biomaterial following diazonium modification. The azobenzene compound formed due to the reaction exhibited a strong absorption peak at 355 nm for the diazotized SF biomaterial, whereas no such peak was observed for the untreated silk control (Figure 3A). The percentage of tyrosine residue

modification with an azo compound within the SF biomaterial was calculated using Beer−Lambert's law. The respective azo concentration of the diazotized silk was calculated using a molar extinction coefficient of 22,000 M^{-1} cm^{-1}, and the absorbance at 347 nm was 2.5×10^{-5} mM. The corresponding
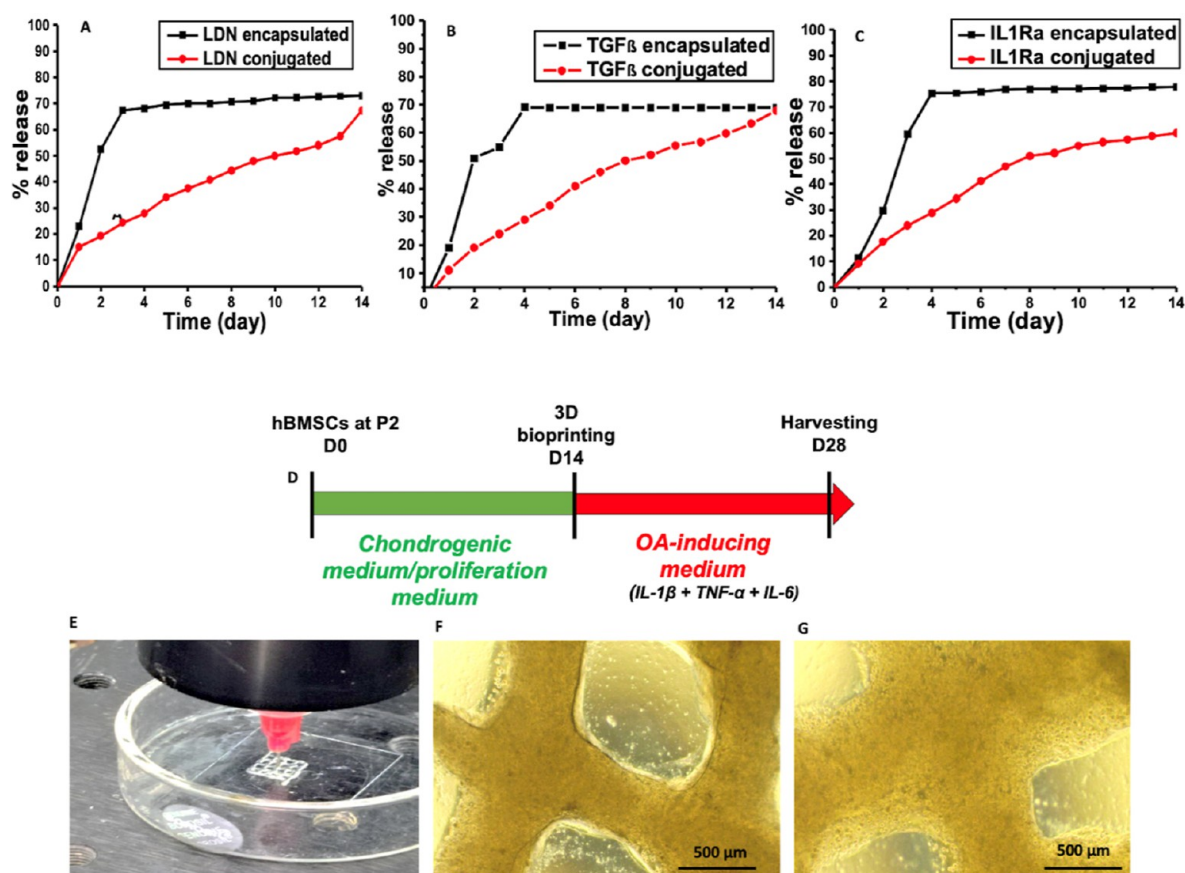
Figure 4. (A) Release profile of LDN193189 in chemically conjugated and encapsulated form, (B) release profile of TGFβ in chemically conjugated and encapsulated form, (C) release profile of IL1Ra in chemically conjugated and encapsulated form, (D) experimental timeline, and (E−G) 3D bioprinting and evaluation of bioprinted constructs at day 3 using bright-field microscopy demonstrating perfect grid structure with homogeneous cell distribution throughout the construct.

percentage of azo-modified tyrosine residues was estimated at 76.9%, considering 115 tyrosine residues per molecule (Table 2).

3.2.3. Rheological Characterization.
The rheological profile of the respected chemically modified SF-G bioinks was performed to analyze the effect of these chemical modifications on the printability of the bioinks (Figure 3). The viscosity vs shear rate curve performed at 25 °C demonstrated a characteristic shear thinning behavior for both the experimental groups (SF-G-CyCl and SF-G-Diazo) and the control group (SF-G) (Figure 3B). An earlier investigation[59] calculated that the shear rate at the tip of the cylindrical 210 μm nozzle is within the range of 198.7−386.7 s^{-1}. Thus, from the figure, the viscosity drop at 216 s^{-1} for all the groups was calculated to be 90.15% for the SF-G-Diazo group, whereas it was 73.2% for the SF-G-CyCl group compared to 60.35% in the untreated SF-G control. Therefore, all the chemically modified bioinks showed adequate printability characteristics and decreased viscosity profile upon the increasing shear rate. The gelation kinetics of the respective chemically modified hydrogels were evaluated from time sweep analysis, and the crossover point of storage modulus (G') and loss modulus (G'') is termed as the "gelation time". The gelation time of SF-G-untreated one was evaluated as 10.2 min, whereas for CyCl-modified and Diazo-modified ones, it is 8.5 and 7.67 min, respectively (Figure 3C− E). The printability characteristics were evaluated by calculating the spreading ratio and the printability index. The spreading ratio was highest for the SF-G-Diazo group (1.51 ± 0.177), followed by the SF-G-CyCl group (1.43 ± 170). A spreading ratio of 1 is considered an ideal condition for ensuring the highest printability, which is approximately observed in the unmodified SF-G group (1.28 ± 0.028) (Figure 3F−I). The printability index value was, however, close to 1 for all the experimental groups, rendering no to negligible interference of the chemical modifications on the printability characteristics of the bioink (Figure 3J−L).

3.2.4. In Vitro Release Kinetics.
The in vitro release kinetics of the small molecule and growth factors from the respective chemically modified SF biomaterial strongly corroborated their chemical conjugation with the biomaterial and were evaluated for 14 days. The release profile of the individual chemically conjugated SF matrices was compared to the direct small molecule encapsulated matrices and SF control. The conjugated LDN193189 and TGFβ3 from the CyCl-modified SF-G biomaterial demonstrated sustained release kinetics for 14 days with 67.4 and 67.9% releases, respectively. In contrast, the direct encapsulated group showed a burst release of 67% within day 3 for LDN and 69.1% within day 4 for TGFβ3. The release profile of IL1Ra from the diazo-modified SF-G also demonstrated a sustained release profile with 59.9% release within day 14. Such a controlled release pattern confirms the successful chemical attachment of the small molecules (LDN193189, IL-1Ra) and growth factor (TGFβ3) with the SF-G biomaterial (Figure 4A−C).
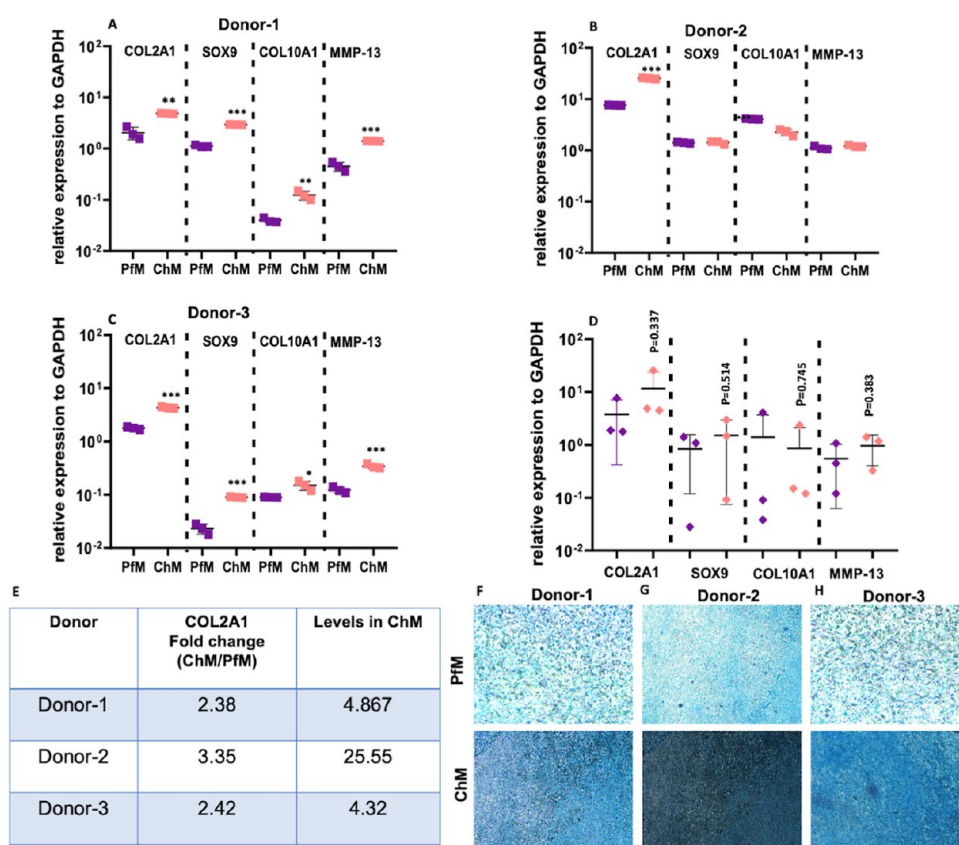
Figure 5. Evaluating the chondrogenesis profile of hBMSCs from three different donors primed with chondrogenic differentiation medium (ChM) for 14 days in monolayer against a proliferation medium (PfM) control (A–C) gene expression analysis of chondrogenic (COL2A1 and SOX9) and hypertrophic (COL10A1 and MMP-13) markers using qPCR for donor-1, donor-2, and donor-3, respectively. The gene expression data were normalized to day 1 values, (D) donor-to-donor variation of gene expression data, (E) COL2A1 expression levels of the different donors, and (F–H) Alcian blue staining depicting enhanced GAG deposition in ChM samples than in PfM after 14 days of the culture period. All experiments were carried out in triplicates ($n = 3$), and the statistical analysis was represented as * ($p \leq 0.033$), ** ($p \leq 0.002$), *** ($p \leq 0.001$), and **** ($p < 0.0001$).

3.3. Visualization of the 3D Bioprinted Constructs.

Bright-field microscopy evaluation demonstrated (a) interfilament pore dimension and (b) homogeneous cell distribution throughout the 3D bioprinted constructs. The interfilament pore morphology post 3D bioprinting of cell-laden SF-G bioink demonstrated a square geometry with an efficient stacking of layers, ensuring the structural stability of the constructs during the 14 days of culture. Such prominent interfilament pore morphology allows uniform distribution of nutrients and gases throughout the construct. Additionally, from the bright-field microscopy images, it is evident that the encapsulated chondrogenic hBMSCs were homogeneously distributed throughout the construct, assuming a round morphology embedded in the matrix, a typical characteristic of chondrocytes in the native tissue microenvironment (Figure 4E–G).

3.4. Evaluation of Chondrogenesis Post 14 days of hBMSC Chondrogenic Differentiation.

The hBMSCs from three different donors were cultured in chondrogenic differentiation media for a period of 14 days in a monolayer, and the extent of chondrogenic trait induction was evaluated using the qPCR method. A set of four genes was employed, consisting of two chondrogenic genes (COL2A1 and SOX9) and two hypertrophic marker genes (COL10A1 and MMP-13). After 14 days of culture, the hBMSCs demonstrated a spike in the expression of the chondrogenic marker genes COL2A1 and

SOX9 for all three donors when compared with their respective proliferative medium hBMSC control. The donor-2 hBMSCs demonstrated the highest COL2A1 gene expression (3.4-fold, $p < 0.001$), whereas donor-3 hBMSCs displayed the highest SOX9 expression (5.1-fold, $p < 0.001$) against the proliferation medium control. A negligible expression of hypertrophic marker COL10A1 and matrix-degrading marker MMP-13 elucidated the antihypertrophic characteristics of the chondrogenically differentiated hBMSCs with variation among the three donors (Figure 5A–D). Among them, donor-2 hBMSCs depicted a 1.6-fold ($p < 0.001$) decrease in COL10A1 expression, whereas donor-1 and donor-3 hBMSCs illustrated a 2.6-fold and 1.6-fold spike in COL10A1 expression, respectively, against PfM control. Alcian blue staining demonstrated comparatively dense staining in the chondrogenic samples of all three donors compared to the proliferation medium control, signifying significant proteoglycan deposition by the chondrogenically differentiated hBMSC.

3.5. Gene Expression Analysis.

The 3D bioprinted constructs constituting small molecules and growth factor conjugated SF-G constructs encapsulated with chondrogenically differentiated hBMSCs were incubated in the OA-inducing medium (HyM + INFL). Although the chondrogenesis profile of the embedded hBMSCs was already analyzed, the next primary objective was to investigate the maintenance of this stable chondrogenic phenotype in a 3D microenviron-
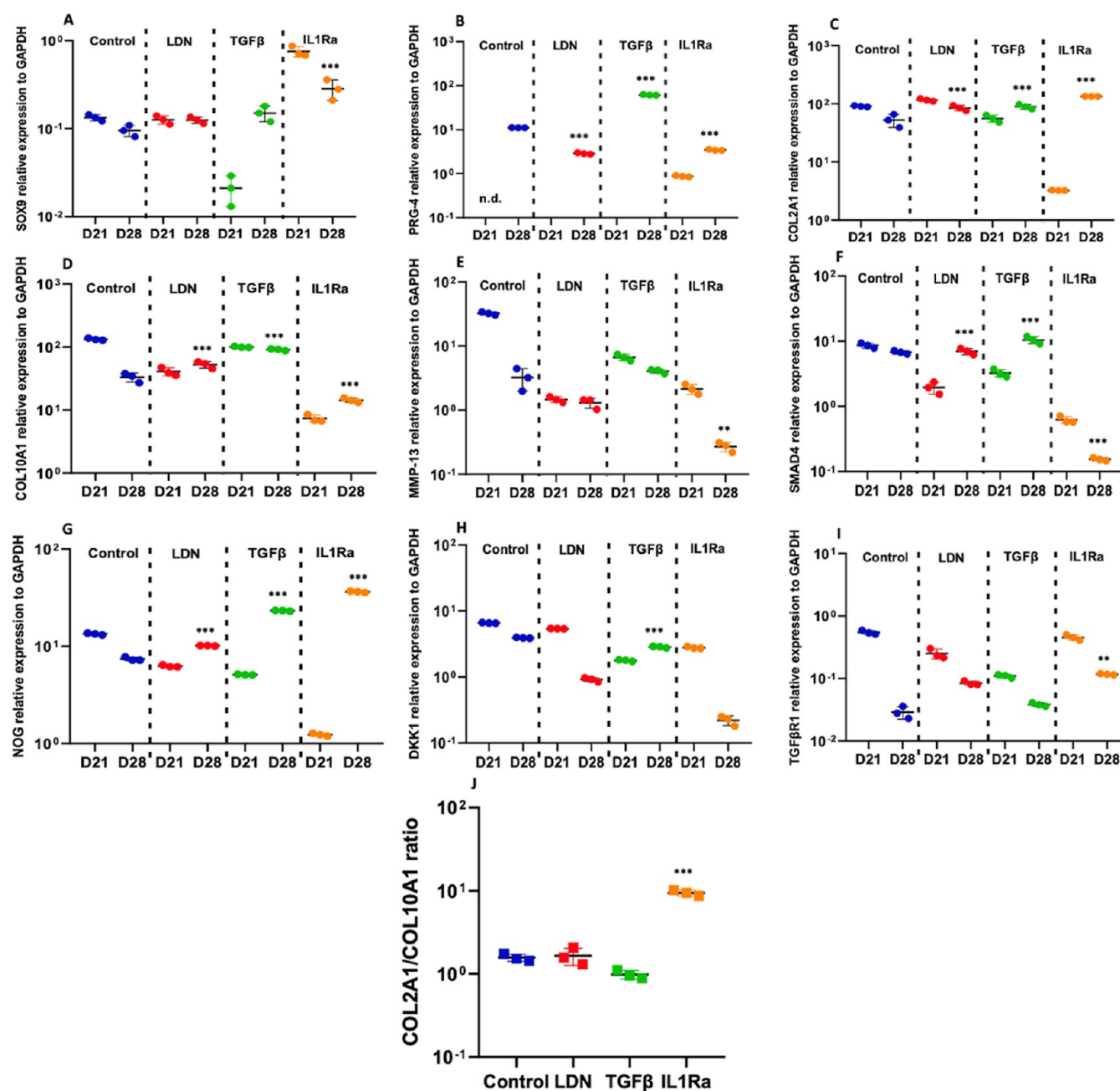
Figure 6. (A–J) Gene expression analysis of chondrogenic (SOX9, PRG-4, and COL2A1), hypertrophic (COL10A1 and MMP-13), signaling pathway (SMAD-4, NOG, DKK1, and TGFβR1) markers and COL2A1/COL10A1 ratio of donor-2 3D bioprinted constructs at day 28 of inflammatory culture incubation. The gene expression data were normalized to day 1 values; n.d.: under the expression level. All experiments were carried out in triplicates ($n = 3$), and the statistical analysis was represented as * ($p \leq 0.033$), ** ($p \leq 0.002$), *** ($p \leq 0.001$), and **** ($p < 0.0001$).

ment (SF-G matrix) during its course of culture in an OA-inducing medium (Figure 6). The gene expression data of only donor-2 have been included in the main article, whereas donor-1 and donor-3 are included in the Supporting Information. The gene expression data corresponding to the selected chondrogenic, hypertrophic, and signaling pathway marker genes (Table 1) were highly variable and donor-dependent, as mentioned in Table 3.

The maintenance of chondrogenic traits under an OA-inducing microenvironment was examined through the expression profile of the chondrogenic markers **SOX9**, **PRG-4**, and **COL2A1** genes.

The expression profile of early-stage chondrogenic marker **SOX9** showed a spiked increase for SF-G-IL1Ra for an early time point (7.1-fold, $p = 0.0005$) that declined after reaching the final time point for donor-2 (Figure 6A). The trend was similar for donor-3 but was reversed for donor-1 with an increase in SOX9 expression level from day 21 to day 28 (Supporting Information Figures 1A and 2A). The expression level of **proteoglycan 4** (**PRG-4**) demonstrated an elevated profile in the SF-G-TGFβ group for donor-2 at day 28 (5.5-fold, $p < 0.001$) (Figure 6B). However, the SF-G-LDN group for all three donors displayed a negligible PRG-4 expression on the final time point (Supporting Information Figures 1B and

Table 3. Similarity Percentage between the Donors Concerning the Gene Expression Values

genes	experimental groups	donor-1 vs donor-2 (%)	donor-2 vs donor-3 (%)	donor-1 vs donor-3 (%)
COL2A1	control	4.98	93.94	4.46
	LDN	27.40	96.06	29.24
	TGFβ	24.21	82.37	32.87
	IL1Ra	3.93	26.54	23.16
SOX9	control	4.97	35.28	20.44
	LDN	36.65	47.02	12.92
	TGFβ	51.76	34.05	13.32
	IL1Ra	31.93	71.48	19.37
COL10A1	control	0.95	34.55	4.43
	LDN	5.32	39.94	1.36
	TGFβ	1.92	67.56	0.99
	IL1Ra	15.86	7.46	0.67
MMP-13	control	4.38	17.25	38.55
	LDN	0.00	0.00	10.97
	TGFβ	6.86	0.79	19.92
	IL1Ra	0.00	90.61	0.00
SMAD-4	control	6.31	3.45	69.74
	LDN	1.50	5.94	39.51
	TGFβ	9.68	50.89	24.63
	IL1Ra	82.88	49.62	37.85
NOG	control	33.54	28.33	6.44
	LDN	49.30	14.81	5.10
	TGFβ	33.23	20.30	4.40
	IL1Ra	95.69	3.16	3.42
DKK1	control	0.00	58.01	0.00
	LDN	0.00	0.00	12.43
	TGFβ	10.60	0.00	0.00
	IL1Ra	0.00	0.00	0.00
PRG-4	control	0.00	43.89	0.00
	LDN	30.74	85.05	38.96
	TGFβ	3.12	0.00	0.00
	IL1Ra	79.61	24.67	35.05
TGFβR1	control	0.00	0.00	0.00
	LDN	0.00	14.19	0.00
	TGFβ	0.00	1.24	0.00
	IL1Ra	0.00	7.92	0.00

2B). Under the influence of the OA-inducing medium, the expression level of **COL2A1** was significantly higher in all three experimental groups of donor-2, with the highest expression in the SF-G-IL1Ra group (2.6-fold, $p < 0.001$) (Figure 6C). The expression profiles of COL2A1 at the final point for donor-1 and donor-3 (Supporting Information Figures 1C and 2C) depicted successful synthesis of the hyaline cartilage-specific matrix when cultured in an OA-inducing medium.

The induction of chondrogenic hypertrophy was assessed with the gene expression profile of **COL10A1** and matrix catabolism marker **MMP-13** under inflammatory hypertrophic conditions. The COL10A1 expression of SF-G-IL-1Ra depicted a 2.6-fold ($p < 0.001$) decrease than SF-G control at day 28 for donor-2. Conversely, the SF-G-LDN (1.7-fold, $p < 0.001$) and SF-G-TGFβ (2.7-fold, $p < 0.001$) groups of donor-2 showed an enhanced COL10A1 expression than the control at day 28 (Figure 6D). All the experimental groups of donor-1 depicted an increasing trend in COL10A expression at day 28 against the control group, illustrating the onset of chondrocyte hypertrophy (Supporting Information Figure

1D). The OA catabolic marker **MMP-13** depicted a decrease in expression from day 21 to day 28 for all the experimental groups of donor-2 with SF-G-IL1Ra, showing the maximum decrease (6.4-fold, $p < 0.001$) (Figure 6E). In contrast, the MMP-13 expression profile in the SF-G-IL1Ra group of donor-1 (66.9-fold, $p < 0.001$) and donor-3 (8.0-fold, $p < 0.001$) depicted an increasing trend at day 28 (Supporting Information Figures 1E and 2E), whereas it was the reverse for donor-2 (14.6-fold, $p < 0.001$). Thus, expression profiles of hypertrophic markers are highly donor-dependent.

A wide array of signaling pathways is associated with the maintenance of cartilage homeostasis. The analysis of **SMAD-4** gene expression is essential to unravel the activation or deactivation details of the BMP signaling downstream target. For all three donors, there is a negligible expression of the SMAD-4 gene in the SF-G-IL1Ra group with donor-2 (44.6-fold, $p < 0.001$) (Figure 6F) and donor-3 (319-fold, $p < 0.001$) (Supporting Information Figure 2F) showing the maximum decrease at day 28 compared to the control. Despite conjugating BMP-signaling inhibitor LDN193189 to the SF-G biomaterial, the SF-G-LDN group displayed an increased SMAD-4 expression irrespective of the donor.

The expression profile of BMP signaling inhibitor **Noggin** (**NOG**) at day 28 under inflammatory hypertrophic culture condition was also highest in the SF-G-IL1Ra group (4.9-fold, $p < 0.001$), followed by the SF-G-TGFβ group (3.1-fold, $p < 0.001$), compared to the control for donor-2 (Figure 6G). The SF-G-LDN group, however, displayed minimum NOG expression for all three donors at day 28 compared to the other experimental groups. Thus, BMP signaling inhibition supported the maintenance of the articular cartilage phenotype in the SF-G-IL1Ra group with adequate control over chondrocyte hypertrophy and inhibited inflammation through IL1Ra. The expression profile of Wnt signaling pathway inhibitor **Dickkopf-1** (**DKK1**) is important to understand the status of the Wnt/β-catenin pathway in regulating chondrogenesis. The highest DKK1 expression was observed in the SF-G control group for donor-2 (Figure 6H) and donor-3 (Supporting Information Figure 2H), implying significant inhibition of the Wnt/β-catenin signaling cascade. However, negligible expressions of DKK1 in the SF-G-IL1Ra group at day 28 for all three donors significantly demonstrated the elevated activation of the Wnt/β-catenin pathway, thus exhibiting the highest chondrogenic characteristics. The expression profile of the **transforming growth factor beta receptor 1** (**TGFβR1**) gene indicates the activation of the TGFβ signaling cascade, a key modulator of chondrogenesis. The maximum expression level was shown in the SF-G-IL-1Ra group for donor-2 (5.2-fold, $p < 0.002$) (Figure 6I) and SF-G-TGFβ group for donor-3 (34.3-fold, $p < 0.001$) (Supporting Information Figure 2I). No expression of the TGFβR1 gene was observed in any experimental groups of donor-1.

The COL2A1/COL10A1 mRNA ratio reached the highest levels in the IL1Ra group (9.4), indicating that IL1Ra, among the other tested bioactive molecules, was more effective in inducing the formation hyaline-like cartilage by the hBMSCs, even in the presence of OA-triggering factors (Figure 6J).

3.6. Biochemical Analyses. The glycosaminoglycans comprise the main component of articular cartilage tissue and, when covalently bound to the core proteins, are termed proteoglycans (aggrecan). The levels of these GAGs vary with different layers of the hyaline cartilage and are highly reduced during OA progression under the inflammatory microenviron-

K

ment. The nitric oxide and lipid peroxidation are directly related to the pathophysiology of OA manifestation. The nitrite oxide allows for sequestration of the pro-inflammatory factor NF-kB, thereby creating an inflammatory niche. The chondrocyte lipid peroxidation, on the other hand, contributes to cartilage aging with the breakdown of the surrounding cartilage ECM, thereby promoting OA. Thus, evaluating the TNO content, total nitrite content, lipid peroxidation profile, and total proteoglycan content at the final time point (day 28) for all the experimental and control groups under inflammatory culture conditions is important to analyze the specific role of IL1Ra in arresting chondrocyte hypertrophy (Figure 7 for donor-2) and Supporting Information Figure 3 for donor-1 and donor-3.
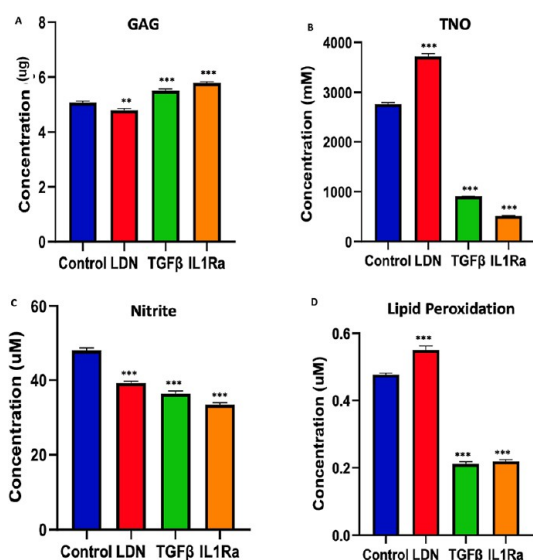

Figure 7. (A–D) Biochemical estimation of (A) proteoglycan content (DMMB), (B) TNO, (C) total nitrite content (nitrite), and (D) lipid peroxidation profile of donor-2 3D bioprinted constructs at day 28 of inflammatory culture incubation. All experiments were carried out in triplicates ($n = 3$), and the statistical analysis was represented as * ($p \leq 0.033$), ** ($p \leq 0.002$), *** ($p \leq 0.001$), and **** ($p < 0.0001$).

3.6.1. DMMB Assay. The 1,9-dimethyl methylene blue (DMMB) assay is used to quantify the deposited sulfated glycosaminoglycan (sGAGs) by the encapsulated hBMSCs. Under inflammatory conditions, the highest sGAG deposition was observed in the SF-G-IL1Ra group for donor-2 (5.78 ± 0.05 μg, $p < 0.001$), followed by the SF-G-TGFβ group (5.5 ± 0.07 μg, $p < 0.001$) (Figure 7A). The highest sGAG accumulation of donor-1 and donor-3 at day 28 is also observed in the SF-G-IL1Ra group (4.9 ± 0.3415 μg, $p < 0.001$) and (7.07 ± 0.07 μg, $p < 0.001$), respectively, followed by SF-G-LDN (4.05 ± 0.1714 μg, $p = 0.069$) of donor-2 and SF-G-LDN (6.81 ± 0.01 μg, $p < 0.001$) of donor-3 compared to the SF-G control (Supporting Information Figures 3A,B).

3.6.2. TNO Content. The TNO content is an evident catabolic regulator of OA progression, which showed a higher release concentration of 3717 ± 57.91 μM ($p < 0.001$) in the SF-G-LDN group of donor-2, while SF-G-IL1Ra showed the lowest TNO content (511.3 ± 7.84 μM, $p < 0.001$) (Figure 7B). Under inflammatory conditions for donor-1, a maximum TNO content of 641.6 ± 24.36 μM ($p < 0.001$) was observed in the SF-G-TGFβ group followed by the SF-G-IL1Ra group (410.6 ± 0.7049 μM, $p = 0.003$) compared to the SF-G control

(464.9 ± 6.665 μM) group (Supporting Information Figure 3C). The LDN conjugated SF-G group of donor-1 depicted the lowest release of nitric oxide (113.8 ± 4.997 μM, $p < 0.001$), signifying minimum tendency toward OA progression. The TNO content profile of donor-3 followed a similar trend as donor-1, with the highest TNO content released by the SF-G-TGFβ group (6167 ± 103.9 μM) and the lowest by SF-G-IL1Ra group (4674 ± 26.76 μM) at day 28 (Supporting Information Figure 3D).

3.6.3. Total Nitrite Content. Estimating the total nitrite content released by the encapsulated chondrogenic hBMSCs during its incubation under OA-mimicking conditions also significantly contributes to the pathogenesis of OA. Under inflammatory conditions, for donor-2, the highest nitrite ion release at day 28 is observed in the SF-G control group (48.08 ± 0.58 μM, $p < 0.001$), followed by SF-G-LDN (39.28 ± 0.41 μM, $p < 0.001$), SF-G-TGFβ (36.37 ± 0.8 μM, $p < 0.001$), and SF-G-IL1Ra group (33.40 ± 0.6 μM, $p < 0.001$) (Figure 7C). However, for donor-1, the SF-G-TGFβ group demonstrated the highest release of nitrite ions of 24.48 ± 8.335 μM ($p = 0.315$) at day 28 compared to the SF-G control group. Additionally, the SF-G-IL1Ra and SF-G-LDN groups demonstrated the lowest release profile of nitrite ions with 13.01 ± 4.302 μM ($p > 0.99$) and 16.01 ± 5.625 μM ($p > 0.99$), respectively (Supporting Information Figure 3E). However, similar to donor-1, the highest total nitrite content was observed in the SF-G-TGFβ group (74.02 ± 1.07 μM, $p < 0.001$) and lowest in the SF-G-IL1Ra group (61.73 ± 1.17 μM, $p = 0.002$) at day 28 for donor-3 (Supporting Information Figure 3F).

3.6.4. Lipid Peroxidation Profile. The estimation of the lipid peroxidation profile is a clear indicator of oxidative stress in cells under the influence of various exogenic stress measured by quantifying its decomposition by the byproduct thiobarbituric acid reactive substances (TBARS). Therefore, a higher concentration of TBARS illustrates enhanced cell membrane degradation and oxidative stress in the encapsulated cells. The highest lipid peroxidation profile was observed in the SF-G-LDN group (0.55 ± 0.01 μM, $p < 0.001$) and lowest in SF-G-TGFβ (0.21 ± 0.005 μM, $p < 0.001$) and SF-G-IL1Ra (0.21 ± 0.005 μM, $p < 0.001$) at day 28 (Figure 7D). The concentration of TBARS was highest in the SF-G control group of donor-1 under inflammatory conditions, with 0.426 ± 0.055 μM demonstrating the most elevated oxidative stress in the diseased control group (Supporting Information Figure 3G). The SF-G-TGFβ and SF-G-LDN groups, however, displayed a comparative trend of TBARS production with 0.383 ± 0.0321 μM ($p = 0.799$) and 0.38 ± 0.05085 μM ($p = 0.191$), respectively. The minimum cell membrane rupture due to lipid peroxidation was observed in the SF-G-IL1Ra group, with the lowest production of TBARS of 0.213 ± 0.035 μM ($p = 0.001$) on day 28. However, for donor-2 and donor-3, the SF-G control group (0.48 ± 0.005 μM) demonstrated a similar lipid peroxidation profile as the SF-G TGFβ3 group (0.49 ± 0.002 μM, $p = 0.120$) at day 28, depicting the highest loss of cell membrane integrity (Supporting Information Figure 3H).

Thus, from the abovementioned observations, it can be clearly seen that the IL1Ra-conjugated group demonstrated the maximum GAG accumulation with reduced levels of nitrite, TNO, and lipid peroxidation when compared to LDN- and TGFβ3-conjugated groups.

3.7. Protein Expression. Immunostaining was performed to assess chondrogenic and hypertrophic collagen proteins
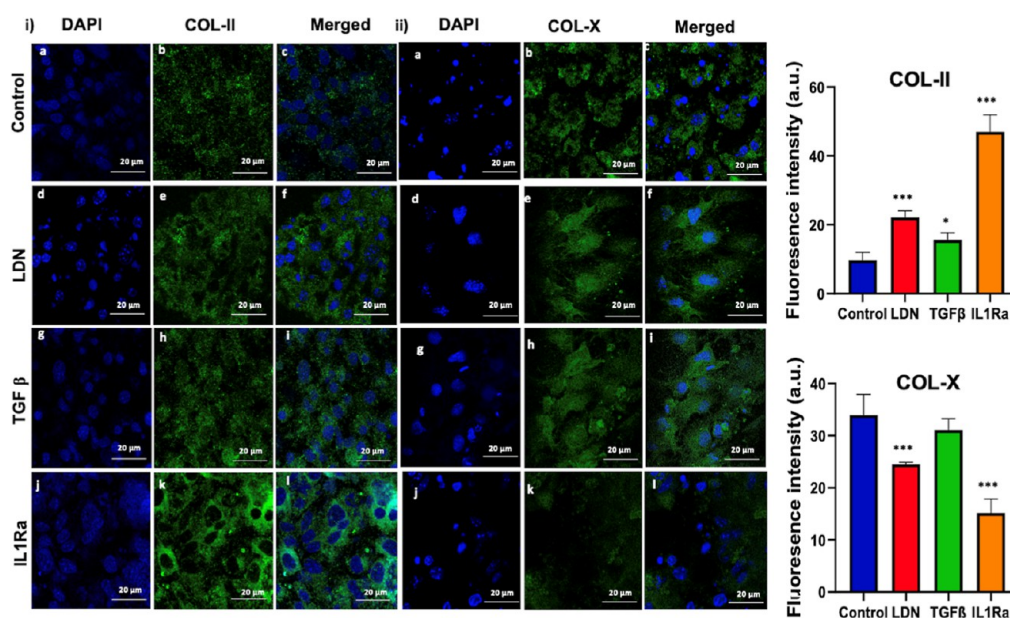
Figure 8. (i)(a−l) COL-II and (ii)(a−l) COL-X protein expression analysis using immunofluorescence. The constructs were incubated with mouse anti-collagen II (5 μg/mL, DSHB) and mouse anti-collagen X (5 μg/mL, DSHB), followed by incubation with secondary antibody antimouse Alexa Fluor 488 (2 μg/mL, Thermo Fisher Scientific) and DAPI (1 μg/mL, Thermo Fisher Scientific). The respective fluorescence intensity was calculated using ImageJ software; the measurements were taken from 5 different regions ($n = 5$), and the statistical analysis represented as * ($p \leq$ 0.033), ** ($p \leq 0.002$), *** ($p \leq 0.001$), and **** ($p < 0.0001$).

(COL-II and COL-X) in the 3D bioprinted constructs as investigated from the respective gene expression profiles. From the gene expression and biochemical estimation data concerning the three donors, the most chondrogenic traits were exhibited by donor-2 hBMSCs. Hence, the donor-2 experimental samples were used for further protein expression using immunostaining. When the BMSC-loaded chemically decorated constructs were incubated in an OA-inducing medium, the expression of **COL-II** protein [Figure 8(i)(a−l)] was comparatively lower in the SF-G control group at the final time point. However, both SF-G-LDN (2.3-fold, $p <$ 0.001) and SF-G-TGFβ (1.6-fold, p = 0.019) depicted adequate COL-II protein expression at day 28 in an OA-inducing medium, illustrating the pro-chondrogenic role of the respective conjugated small molecule and growth factor in stimulating chondrogenesis. Additionally, the SF-G-IL1Ra group demonstrated maximum chondrogenesis with enhanced deposition of COL-II protein at day 28 in the OA-inducing medium (4.9-fold, $p <$ 0.001) compared to the SF-G control. Furthermore, the secreted collagen protein was observed within the pericellular space and in the extracellular matrix, recapitulating the native ECM microarchitecture of articular cartilage tissue.

The expression of **COL-X** protein [Figure 8(ii)(a−l)] depicted the induction of hypertrophic differentiation of the differentiated hBMSCs under both inflammatory hypertrophic culture conditions. The highest COL-X expression was observed in the SF-G-TGFβ group under the influence of inflammatory culture conditions on day 28, akin to the SF-G control group (p = 0.235). The SF-G-LDN group, however, demonstrated a significant COL-X expression under inflammatory hypertrophic conditions, underlining the onset of chondrocyte hypertrophy despite inhibiting the BMP signaling pathway. The SF-G-IL1Ra group under OA-inducing conditions illustrated the lowest level of COL-X expression (2.2-fold, $p <$ 0.001), emphasizing the minimum hypertrophic

maturation of the chondrogenic hBMSCs encapsulated within the chemically decorated SF-G constructs.

3.8. Histological Evaluation. The Safranin-O staining examined the glycosaminoglycan deposition postincubation in OA-mimicking conditions of all the chemically modified experimental groups and SF-G control for 14 days. The SF-G-IL1Ra group demonstrated the maximum glycosaminoglycan deposition, followed by the SF-G-LDN group. The SF-G-TGFβ and SF-G control groups showed an opposite deposition of sGAGs, but it was comparatively less than the SF-G-IL1Ra and SF-G-LDN groups. The Alcian blue staining also depicted sufficient deposition of GAG around the cells, signifying adequate chondrogenesis. The hematoxylin and eosin staining revealed spherical morphology of the cells in all the groups, a typical characteristic of chondrocytes. More evident cell clustering, cell enlargement, as well as higher expression of type X collagen in the SF-G control and TGFβ group evidence in the immunofluorescence data suggests a stronger tendency of the cells in these groups to acquire OA traits once cultured in the OA-inducing medium. Results from qPCR and biochemical analyses confirm these trends. Instead, cells from the SF-G-LDN and SF-G-IL1Ra groups exhibit a less pronounced tendency to acquire these aforementioned OA traits, indicating that LDN and IL-1Ra were effective in counteracting hypertrophic maturation of the cartilaginous tissues under an OA-inducing medium. Thus, all the respective groups demonstrated successful maintenance of chondrogenic phenotype, with SF-G-IL1Ra getting the upper hand (Supporting Information Figure 4).

3.9. GeneMANIA Analysis. To gain insights into how the chosen set of genes collectively function to maintain articular cartilage phenotype, we utilized the Gene MANIA database to predict their interactions with each other. We have chosen five genes that showed upregulated expression in qPCR for the analysis in each experimental group of donor-2. Our investigation revealed a complex network of interactions that
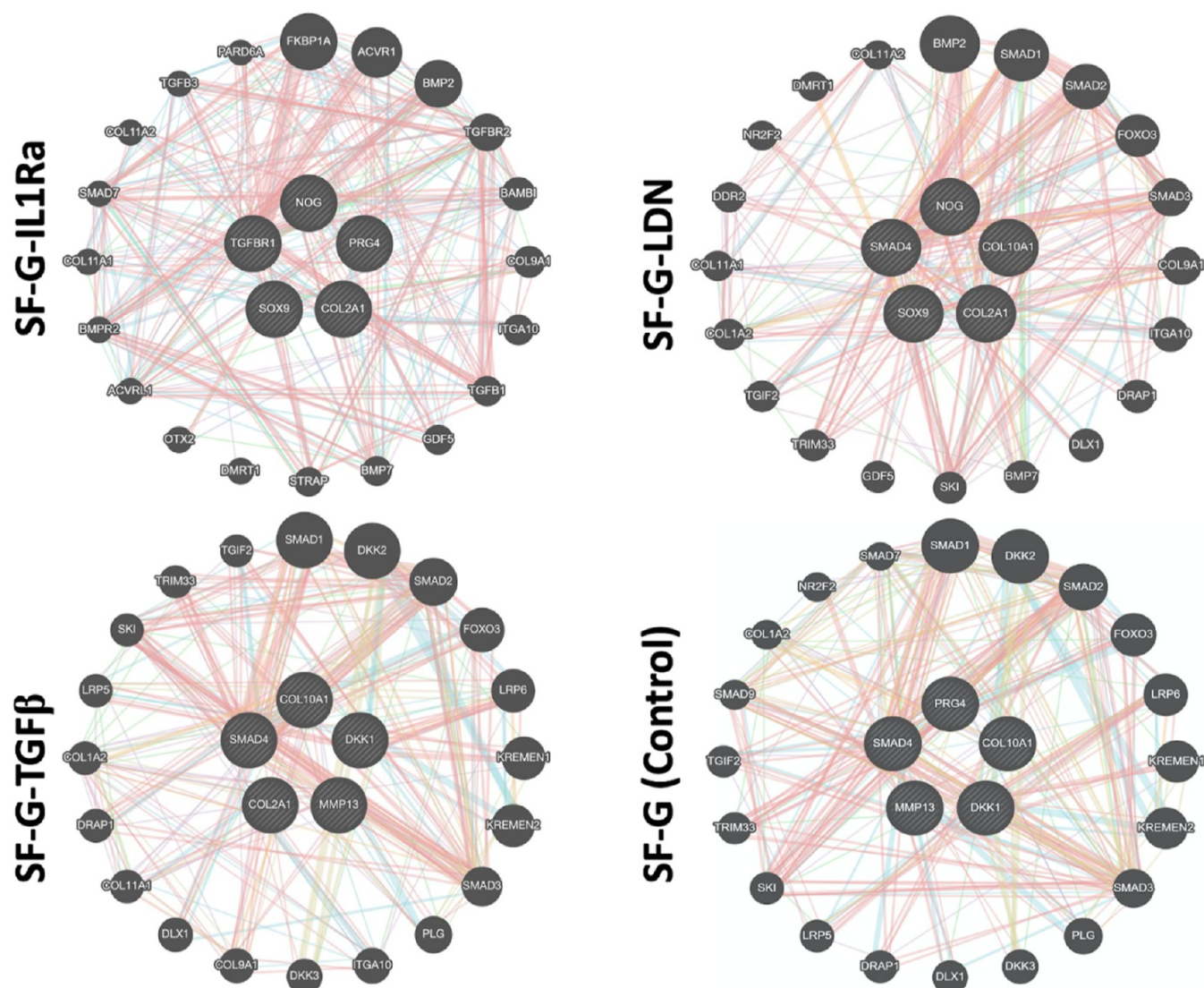
Figure 9. Gene MANIA analysis depicting the correlation and interaction of the input genes with the pool of genes associated with articular cartilage homeostasis. Five upregulated genes (from qPCR analysis) of each experimental group of donor-2 were selected for the interaction study. (**SF-G-IL1Ra**: *NOG*, *PRG4*, *TGFβR1*, *COL2A1,* and *SOX9*; **SF-G-TGFβ**: *COL10A1*, *DKK1*, *MMP13*, *SMAD4,* and *COL2A1*; **SF-G-LDN**: *NOG*, *COL10A1*, *COL2A1*, *SOX9,* and *SMAD4*; **SF-G**: *PRG4*, *COL10A1*, *DKK1*, *MMP13,* and *SMAD4*).

collectively govern the regulation, preservation, and repair of cartilage tissue (Figure 9).

For the control group, COL10A1, DKK1, PRG-4, MMP-13, and SMAD-4 genes were chosen. The COL10A1 engages with MMP13 and DKK1, suggesting its role in regulating extracellular matrix composition and tissue remodeling during endochondral bone formation. PRG4, also known as proteoglycan 4, influences the cartilage extracellular matrix by interacting with COL10A1 and PLG, thereby contributing to joint lubrication and protection. MMP13, a matrix metalloproteinase, further aids tissue remodeling by interacting with DKK1 and COL1A2. DKK1 plays a critical role in the Wnt signaling pathway, contributing to cartilage development regulation.

For the LDN group, COL2A1, SOX9, COL10A1, NOG, and SMAD-4 were chosen. COL2A1, a fundamental component of the cartilage extracellular matrix, interacts with various collagens (COL10A1, COL11A1, and COL11A2) and SOX9, emphasizing its role in maintaining the structural integrity and composition of cartilage. SOX9, a master regulator of chondrogenesis, interacts with SMAD3, ITGA10, and FOXO3, signifying its critical role in TGFβ signaling and cell−matrix interactions that shape chondrocyte differentiation and cartilage development. The COL10A1, associated with hypertrophic cartilage, interacts with BMP2, indicating its involvement in chondrocyte differentiation and endochondral ossification.

For the TGFβ3 group, COL2A1, COL10A1, MMP-13, SMAD-4, and DKK1 genes were chosen. MMP13, through its interactions with DKK1, COL10A1, COL11A1, and COL1A2, influences tissue remodeling by regulating the degradation of extracellular matrix components, affecting the composition and integrity of the cartilage matrix. SMAD4 interacts with SMAD2, and TGIF2 plays a pivotal role in mediating TGFβ signaling, which is critical for chondrogenesis by regulating chondrocyte proliferation and differentiation. COL10A1's interactions with COL1A2, COL11A1, PLG, and COL9A1 indicate its involvement in maintaining extracellular matrix composition, influencing tissue integrity and development.

For the IL1Ra group, COL2A1, SOX9, NOG, TGFβR1, and PRG-4 genes were chosen. GFBR1 interacts with ACVR1 and GDF5, reflecting the intricate interplay essential for the regulation of chondrogenesis. NOG, through its interaction with BMP2, prevents excessive BMP signaling during cartilage development. COL2A1, as a key component of the cartilage extracellular matrix, interacts with other collagens (COL11A1, COL11A2, and COL9A1) and SOX9, emphasizing its role in maintaining structural integrity and supporting chondrogenesis.

4. DISCUSSION

With the current progression of osteoarthritis as a degenerative joint disorder affecting millions of lives worldwide, cartilage biologists and tissue engineers have been relentlessly making efforts to fabricate tissue-engineered articular cartilage equivalent as a long-time regenerative therapy. However, even after 40 years of arduous research, developing a clinically relevant articular cartilage graft for load-bearing joints remains a major hitch.[53−55] Therefore, our paper extensively elucidated the regulatory role of selected small molecule signaling pathway regulators in maintaining stable articular cartilage phenotype in an OA-mimicking microenvironment when covalently conjugated with our proprietary SF-G bioink.

Earlier studies by different research groups have shown that the exogenous addition of cytokines and growth factors in a culture medium minimizes the bioavailability of the biochemical regulators to the surrounding cells due to their shorter half-life[60,61] and making the process expensive with frequent replenishment. As a result, different strategies corresponding to immobilization or surface functionalization of the growth factors have been adopted. Therefore, first, we wanted to confirm our covalent conjugation strategy of the small molecules with SF biomaterial and their subsequent effect on the rheology and overall printability characteristics of our SF-G bioink. For covalent attachment of the small molecules and growth factors (LDN193189, TGFβ3, and IL1Ra) to the SF biomaterial, we have adopted two chemical modification strategies: (a) cyanuric chloride (CyCl) coupling (LDN193189 and TGFβ3) and (b) diazonium coupling (IL1Ra). Initially, a molecular modeling approach suggested the above-mentioned strategies of covalent conjugation of LDN193189, TGFβ3, and IL1Ra as the most effective method to chemically decorate our SF biomaterial. The stability of the chemically modified SF complexes was further justified using the Ramachandran plot. The hydrophobic interactions between the respective amino acid residues form the hydrophobic core, whereas the electrostatic interaction through salt bridge formation authenticated the structural integrity of the formed chemical conjugates. Furthermore, the disulfide linkages via cysteine residues in SF-Diazo-IL1Ra and the cyclic structure of proline residues in SF-CyCl-LDN corresponded to the additional structural stability of the complexes. Experimentally, ATR-FTIR successfully confirmed the CyCl and diazo modification of SF, respectively, for further conjugation of respective signaling pathway regulators. An increase in beta-sheet content was also reported after the subsequent chemical modification of the SF biomaterial. Such findings underline the regulatory role of the random coil to β-sheet transition in silk to initiate 3D hydrogel network formation.[62] Still, challenges about abrupt or maximum release within a short period limit their application for long-term tissue maturation protocols.[63−65] Therefore, our advanced bioconjugation strategy over exogenous addition or direct adsorption of the small molecule mediators exhibited a sustained release profile for 14 days, thereby allowing for overall increased bioavailability and bioactivity to the embedded cells.

Further, we wanted to analyze whether the cyanuric chloride and diazonium coupling modification altered the rheological profile of the SF-G blend, thereby influencing the overall printability of the bioink. It is well ascribed in our previous studies that the addition of gelatin to SF encompasses shear thinning behavior to the composite bioink and imparts faster gelation characteristics besides providing cell binding motifs.[8,66] The extensive rheological analysis of our chemically modified bioink demonstrated a shear thinning behavior, an optimum gelation time (~8 min), a spreading ratio of ~1, and a printability index close to 1. Thus, it can be rightly concluded that the chemical modifications did not significantly alter the rheological profile and printability properties of the SF-G bioink.

One of the major milestones of the study was to assess whether the 3D bioprinted constructs could maintain the stable chondrogenic phenotype while simultaneously inhibiting chondrocyte hypertrophy when cultured in a hypertrophic medium. The gene expression analysis of the chondrogenic markers SOX9, PRG-4, and COL2A1 gene depicted the IL1Ra conjugated group as the best condition to maintain stable chondrogenic properties for all three donors compared to the SF-G control at day 28. Further, high levels of lubricin gene PRG-4 expression and downregulated Wnt pathway negative regulator DKK1 expression in the SF-G-IL1Ra group on day 28 for all three donors corroborated the pro-chondrogenic attributes of SF-G-IL1Ra group in maintaining stable chondrogenic phenotype when primed with inflammatory hypertrophic culture conditions for a period of 14 days. The COL2A1 and SOX9 genes are among the major hallmarks of chondrogenic differentiation, with SOX9 regulating the expression of the COL2A1 gene.[67] PRG-4, or lubricin, is generally deposited in the thin superficial layer of hyaline cartilage and shields the tissue against the onset of hypertrophic maturation.[68] There are also reports that suggest that neutralizing the function of DKK1 in human MSCs and chondrocytes significantly enhanced the GAG and COL-II deposition levels.[69] This can be matched with our results of the SF-G-LDN and SF-G-TGFβ groups of respective donors exhibiting DKK1 expression parallelly with an enhanced COL2A1 expression and GAG deposition. The inhibition of chondrocyte hypertrophy by the small molecule signaling pathway regulators was validated with the expression profiles of the hypertrophic and its associated signaling pathway markers COL10A1, MMP-13, NOG, and SMAD-4. The IL1Ra group successfully demonstrated the lowest expression of COL10A1, MMP-13, and SMAD-4, whereas an upregulated expression of NOG signified maximum inhibition of the BMP signaling pathway. Thus, the SF-G-IL1Ra group demonstrated an upper hand in illustrating articular cartilage phenotype with maximum inhibition of chondrocyte hypertrophy under inflammatory conditions.

However, an enhanced expression profile of COL10A1 is observed under inflammatory conditions in LDN and TGFβ3 groups, especially for donor-1 and donor-2. The presence of hypertrophic characteristics in chondrogenically differentiated BMSCs despite treatment with LDN193189 has been elucidated by Franco et al.[70] Furthermore, it can also be attributed to the dual functionality role of TGFβ in promoting

chondrogenesis and chondrocyte hypertrophy and their intricate mechanistic crosstalk that mediates the process.[71] The expression of BMP signaling downstream target SMAD4 in the TGFβ3 group of all three donors demonstrates the signaling crosstalk between the BMP signaling pathway and the TGFβ cascade.[72] The evidence for this mechanistic signaling crosstalk lies in the expression of the TGFβR1 gene in the SF-G-LDN group and the simultaneous expression of the BMP signaling inhibitor NOG gene in the SF-G-TGFβ group for all three donors. However, the expression pattern is complementary, with the NOG gene increasing its mRNA levels from day 21 to day 28, whereas the TGFβR1 gene exhibits a declining trend. Therefore, it can be hypothesized that in the presence of small molecules and growth factors, a higher level of BMP signaling inhibition and a lower level of TGFβ signaling activation are required to support stable maintenance of articular cartilage phenotype. A noteworthy observation is the steady expression of SMAD4 despite the conjugation of BMP signaling inhibitor LDN193189 in the SF-G-LDN group of donor-2, necessitating the presence of a BMP signaling cascade in maintaining stable hyaline cartilage phenotype. Existing reports suggest that activation of BMP signaling cascades through various BMP isoforms is necessary for chondrogenic differentiation.[73,74]

The last and final milestone was to analyze the donor-to-donor variation between the three hBMSC donors concerning the chondrogenic and hypertrophic gene expression profile (Supporting Information Figure 5A−C). Among the three donors, donor-2 demonstrated more plausible chondrogenic traits than donor-1 and donor-3 (Figure 6 and Supporting Information Figures S1 and S2). This was further supported by SOX9, PRG-4, and BMP signaling inhibitor NOG gene expression, further corroborating the pro-chondrogenic characteristics of donor-2 over the other two donors. Thus, it can be rightly concluded that donor-2 hBMSCs post chondrogenic differentiation showed an upper hand in maintaining a stable hyaline cartilage phenotype over donor-1 and donor-3 when incubated in an OA-inducing medium. The COL-II protein expression data of donor-2 experimental groups also revealed the added advantage of encapsulated BMSCs in promoting chondrogenesis in vitro. However, if we consider the expression profile of the catabolic marker MMP-13, donor-3 illustrated the maximum expression levels than donor-1 and donor-2 at day 28. Therefore, the experimental samples from donor-3 displayed a strong inclination toward hypertrophic differentiation with enhanced matrix catabolism (Figure 6 and Supporting Information Figures 1 and 2). The similarity index was calculated by evaluating the Euclidian distance of the gene expression values between a pair of donors. The heatmap generated demonstrated the highest similarity index between donor-2 and donor-3 (80.84%), followed by donor-1 and donor-3 (77.57%) and last between donor-1 and donor-2 (53.85%) (Supporting Information Figure 6).

Therefore, our study, for the first time, covalently tethered small molecules and growth factors to the chemically modified SF biomaterial. The covalent conjugation of the small molecules (LDN193189 and IL-1Ra) and growth factor (TGFβ3) to the SF-G bioink increased their bioavailability to the embedded cells through sustained release. It allowed for successful inhibition of hypertrophic maturation of the chondrogenically differentiated BMSCs, besides promoting the maintenance of stable chondrogenic phenotype augmented with the added intrinsic advantage of SF-G biomaterial in

upregulating the pro-chondrogenic Wnt/β-catenin pathway to promote neo-chondrogenesis.[16] Further, it highlighted the necessity and strategies of maintaining stable articular cartilage phenotype under OA-mimicking conditions by focusing on neo-cartilage regeneration under a conventional chondrogenic medium, comparing the observations from three different human BMSC donors. The statistical analysis of the results from the experimental samples of three different hBMSC donors revealed a complex heterogeneity even when compared to a single biomarker for simplification, such that the results from one donor bear zero to nominal resemblance to the results of the other donor. Such donor-to-donor variation hints at utilizing a larger donor cohort to produce biologically robust and clinically relevant conclusions. The advantages of 3D bioprinting concerning the spatiotemporal control of biomaterial deposition added with homogeneous cell distribution and regulated pore dimension of the 3D bioprinted construct provided additional benefits in recapitulating the native cell-ECM interaction of the hyaline cartilage tissue.[75] Furthermore, through this research, we have discussed whether complete inhibition of the BMP signaling cascade will allow for successful chondrogenesis with simultaneous inhibition of chondrocyte hypertrophy or allow for dose- and time-dependent inhibition.

5. CONCLUSIONS

This study is aimed at developing a 3D bioprinted articular cartilage tissue using chemically modified SF-gelatin bioink and hBMSCs that will maintain its stable chondrogenic phenotype under OA-inducing conditions by inhibiting chondrocyte hypertrophy. The SF-G bioink was covalently conjugated with specific pro-chondrogenic (TGFβ3) and antihypertrophic (LDN193189 and IL1Ra) small molecule signaling pathway mediators, which was confirmed both computationally and experimentally. The chemically modified SF-G bioinks were declared printable through a detailed rheological and printability analysis. The chondrogenically differentiated BMSCs of the three donors were encapsulated in already chemically modified SF-G bioinks and 3D bioprinted, followed by incubation in an OA-inducing medium. A detailed qPCR and biochemical analyses followed by immunostaining revealed the upper hand of the SF-G-IL1Ra group of all three donors exhibiting pro-chondrogenic characteristics, while inhibiting hypertrophic differentiation. Additionally, donor-2 displayed maximum chondrogenic traits among the three donors, while donor-3 exhibited the strongest tendency toward hypertrophic differentiation. Such donor-to-donor variation in the data generated hinted at using large-sized donor samples to deduce a more comprehensive conclusion. Furthermore, a futuristic study can be designed where a combination of small molecule inhibitors and growth factors into a single bioink would be utilized to fabricate a cartilage graft with an enhanced propensity to induce hyaline-like cartilage repair in OA joints.

■ ASSOCIATED CONTENT

Data Availability Statement

The data will be available with the corresponding author on reasonable request.

ⓢ Supporting Information

The Supporting Information is available free of charge at https://pubs.acs.org/doi/10.1021/acsami.3c18903.

Additional experimental data of the other two donor hBMSCs, including the histology and donor-to-donor variation analysis of all three donors (PDF)

■ AUTHOR INFORMATION

Corresponding Author

Sourabh Ghosh − *Regenerative Engineering Laboratory, Department of Textile and Fibre Engineering, Indian Institute of Technology Delhi, New Delhi 110016, India;* ⬤ orcid.org/0000-0002-1091-9614; Email: Sourabh.Ghosh@textile.iitd.ac.in

Authors

Nilotpal Majumder − *Regenerative Engineering Laboratory, Department of Textile and Fibre Engineering, Indian Institute of Technology Delhi, New Delhi 110016, India*

Chandrashish Roy − *Regenerative Engineering Laboratory, Department of Textile and Fibre Engineering, Indian Institute of Technology Delhi, New Delhi 110016, India*

Laura Doenges − *Department of Biomedicine, University Hospital Basel, University of Basel, Basel 4031, Switzerland*

Ivan Martin − *Department of Biomedicine, University Hospital Basel, University of Basel, Basel 4031, Switzerland;* ⬤ orcid.org/0000-0001-6493-0432

Andrea Barbero − *Department of Biomedicine, University Hospital Basel, University of Basel, Basel 4031, Switzerland;* ⬤ orcid.org/0000-0001-5252-789X

Complete contact information is available at:
https://pubs.acs.org/10.1021/acsami.3c18903

Notes

The authors declare no competing financial interest.

■ REFERENCES

(1) Sandell, L. J.; Aigner, T. Articular cartilage and changes in Arthritis: Cell biology of osteoarthritis. *Arthritis Res.* **2001**, *3* (2), 107−113.

(2) Finnilä, M.; Karhula, S. S.; Cooper, D. M.; Valkealahti, M.; Joukainen, A.; Miller, D.; Nieminen, H.; Kröger, H.; Korhonen, R. K.; Lehenkari, P. P.; Saarakkala, S. 3D Osteocyte Morphology and Volume of Chondrocyte Clusters Are Modulated with Osteoarthritis Severity. *Osteoarthritis Cartilage* **2018**, *26*, S70.

(3) Karim, A.; Amin, A. K.; Hall, A. C. The Clustering and Morphology of Chondrocytes in Normal and Mildly Degenerate Human Femoral Head Cartilage Studied by Confocal Laser Scanning Microscopy. *J. Anat.* **2018**, *232* (4), 686−698.

(4) Malemud, C. J. Changes in Proteoglycans in Osteoarthritis: Biochemistry, Ultrastructure and Biosynthetic Processing. *J. Rheumatol. Suppl.* **1991**, *27*, 60−62.

(5) Sasazaki, Y.; Seedhom, B. B.; Shore, R. Morphology of the Bovine Chondrocyte and of Its Cytoskeleton in Isolation and in Situ: Are Chondrocytes Ubiquitously Paired through the Entire Layer of Articular Cartilage? *Rheumatology* **2008**, *47* (11), 1641−1646.

(6) Ortega, N.; Behonick, D. J.; Werb, Z. Matrix Remodeling during Endochondral Ossification. *Trends Cell Biol.* **2004**, *14* (2), 86−93.

(7) Bhattacharjee, M.; Coburn, J.; Centola, M.; Murab, S.; Barbero, A.; Kaplan, D. L.; Martin, I.; Ghosh, S. Tissue Engineering Strategies to Study Cartilage Development, Degeneration and Regeneration. *Adv. Drug Deliv. Rev.* **2015**, *84*, 107−122.

(8) Das, S.; Pati, F.; Chameettachal, S.; Pahwa, S.; Ray, A. R.; Dhara, S.; Ghosh, S. Enhanced Redifferentiation of Chondrocytes on Microperiodic Silk/Gelatin Scaffolds: Toward Tailor-Made Tissue Engineering. *Biomacromolecules* **2013**, *14* (2), 311−321.

(9) Chakraborty, J.; Majumder, N.; Sharma, A.; Prasad, S.; Ghosh, S. 3D Bioprinted Silk-Reinforced Alginate-Gellan Gum Constructs for Cartilage Regeneration. *Bioprinting* **2022**, *28*, No. e00232.

(10) Miao, T.; Miller, E. J.; McKenzie, C.; Oldinski, R. A. Physically Crosslinked Polyvinyl Alcohol and Gelatin Interpenetrating Polymer Network Theta-Gels for Cartilage Regeneration. *J. Mater. Chem. B* **2015**, *3* (48), 9242−9249.

(11) Chameettachal, S.; Murab, S.; Vaid, R.; Midha, S.; Ghosh, S. Effect of Visco-Elastic Silk-Chitosan Microcomposite Scaffolds on Matrix Deposition and Biomechanical Functionality for Cartilage Tissue Engineering. *J. Tissue Eng. Regen. Med.* **2017**, *11* (4), 1212−1229.

(12) Radhakrishnan, J.; Subramanian, A.; Sethuraman, S. Injectable Glycosaminoglycan-Protein Nano-Complex in Semi-Interpenetrating Networks: A Biphasic Hydrogel for Hyaline Cartilage Regeneration. *Carbohydr. Polym.* **2017**, *175*, 63−74.

(13) Ruvinov, E.; Tavor Re'em, T.; Witte, F.; Cohen, S. Articular Cartilage Regeneration Using Acellular Bioactive Affinity-Binding Alginate Hydrogel: A 6-Month Study in a Mini-Pig Model of Osteochondral Defects. *J. Orthop. Translat.* **2019**, *16*, 40−52.

(14) Chawla, S.; Kumar, A.; Admane, P.; Bandyopadhyay, A.; Ghosh, S. Elucidating Role of Silk-Gelatin Bioink to Recapitulate Articular Cartilage Differentiation in 3D Bioprinted Constructs. *Bioprinting* **2017**, *7*, 1−13.

(15) Chameettachal, S.; Midha, S.; Ghosh, S. Regulation of Chondrogenesis and Hypertrophy in Silk Fibroin-Gelatin-Based 3D Bioprinted Constructs. *ACS Biomater. Sci. Eng.* **2016**, *2* (9), 1450−1463.

(16) Chawla, S.; Desando, G.; Gabusi, E.; Sharma, A.; Trucco, D.; Chakraborty, J.; Manferdini, C.; Petretta, M.; Lisignoli, G.; Ghosh, S. The Effect of Silk-Gelatin Bioink and TGF-B3 on Mesenchymal Stromal Cells in 3D Bioprinted Chondrogenic Constructs: A Proteomic Study. *J. Mater. Res.* **2021**, *36*, 4051−4067.

(17) Menezes, R.; Sherman, L.; Rameshwar, P.; Arinzeh, T. L. Scaffolds Containing GAG-Mimetic Cellulose Sulfate Promote TGF-β Interaction and MSC Chondrogenesis over Native GAGs. *J. Biomed. Mater. Res. A* **2023**, *111* (8), 1135−1150.

(18) Seda Tığlı, R.; Ghosh, S.; Laha, M. M.; Shevde, N. K.; Daheron, L.; Gimble, J.; Gümüşderelioğlu, M.; Kaplan, D. L. Comparative Chondrogenesis of Human Cell Sources in 3D Scaffolds. *J. Tissue Eng. Regen. Med.* **2009**, *3* (5), 348−360.

(19) Yamaguchi, H.; Swaminathan, S.; Mishina, Y.; Komatsu, Y. Enhanced BMP Signaling Leads to Enlarged Nasal Cartilage Formation in Mice. *Biochem. Biophys. Res. Commun.* **2023**, *678*, 173−178.

(20) Barbero, A.; Grogan, S.; Schäfer, D.; Heberer, M.; Mainil-Varlet, P.; Martin, I. Age Related Changes in Human Articular Chondrocyte Yield, Proliferation and Post-Expansion Chondrogenic Capacity. *Osteoarthritis Cartilage* **2004**, *12* (6), 476−484.

(21) Liebesny, P. H.; Mroszczyk, K.; Zlotnick, H.; Hung, H.-H.; Frank, E.; Kurz, B.; Zanotto, G.; Frisbie, D.; Grodzinsky, A. J. Enzyme Pretreatment plus Locally Delivered HB-IGF-1 Stimulate Integrative Cartilage Repair In Vitro. *Tissue Eng., Part A* **2019**, *25* (17−18), 1191−1201.

(22) Gugjoo, M. B.; Gugjoo, M.; Sharma, G. T.; Aithal, H. P.; Kinjavdekar, P. Cartilage Tissue Engineering: Role of Mesenchymal Stem Cells along with Growth Factors & Scaffolds. *Indian J. Med. Res.* **2016**, *144* (3), 339−347.

(23) Xue, K.; Zhang, X.; Gao, Z.; Xia, W.; Qi, L.; Liu, K. Cartilage Progenitor Cells Combined with PHBV in Cartilage Tissue Engineering. *J. Transl. Med.* **2019**, *17* (1), 104.

(24) Scotti, C.; Tonnarelli, B.; Papadimitropoulos, A.; Scherberich, A.; Schaeren, S.; Schauerte, A.; Lopez-Rios, J.; Zeller, R.; Barbero, A.; Martin, I. Recapitulation of Endochondral Bone Formation Using Human Adult Mesenchymal Stem Cells as a Paradigm for Developmental Engineering. *Proc. Natl. Acad. Sci. U.S.A.* **2010**, *107*, 7251−7256.

(25) Scotti, C.; Piccinini, E.; Takizawa, H.; Todorov, A.; Bourgine, P.; Papadimitropoulos, A.; Barbero, A.; Manz, M. G.; Martin, I. Engineering of a Functional Bone Organ through Endochondral Ossification. *Proc. Natl. Acad. Sci. U.S.A.* **2013**, *110* (10), 3997−4002.

(26) Phornphutkul, C.; Wu, K.-Y.; Gruppuso, P. A. The Role of Insulin in Chondrogenesis. *Mol. Cell. Endocrinol.* **2006**, *249* (1−2), 107−115.

(27) Temu, T. M.; Wu, K.-Y.; Gruppuso, P. A.; Phornphutkul, C. The Mechanism of Ascorbic Acid-Induced Differentiation of ATDC5 Chondrogenic Cells. *Am. J. Physiol. Endocrinol. Metabol.* **2010**, *299* (2), E325−E334.

(28) van der Kraan, P. M.; Blaney Davidson, E. N.; Blom, A.; van den Berg, W. B. TGF-Beta Signaling in Chondrocyte Terminal Differentiation and Osteoarthritis: Modulation and Integration of Signaling Pathways through Receptor-Smads. *Osteoarthritis Cartilage* **2009**, *17* (12), 1539−1545.

(29) Ray, A.; Singh, P. N. P.; Sohaskey, M. L.; Harland, R. M.; Bandyopadhyay, A. Precise Spatial Restriction of BMP Signaling Is Essential for Articular Cartilage Differentiation. *Development* **2015**, *142* (6), 1169−1179.

(30) Chakraborty, J.; Ghosh, S. Cellular Proliferation, Self-Assembly, and Modulation of Signaling Pathways in Silk Fibroin Gelatin-Based 3D Bioprinted Constructs. *ACS Appl. Bio Mater.* **2020**, *3* (12), 8309−8320.

(31) Chawla, S.; Mainardi, A.; Majumder, N.; Dönges, L.; Kumar, B.; Occhetta, P.; Martin, I.; Egloff, C.; Ghosh, S.; Bandyopadhyay, A.; Barbero, A. Chondrocyte Hypertrophy in Osteoarthritis: Mechanistic Studies and Models for the Identification of New Therapeutic Strategies. *Cells* **2022**, *11* (24), 4034.

(32) Chawla, S.; Berkelaar, M. H. M.; Dasen, B.; Halleux, C.; Guth-Gundel, S.; Kramer, I.; Ghosh, S.; Martin, I.; Barbero, A.; Occhetta, P. Blockage of Bone Morphogenetic Protein Signalling Counteracts Hypertrophy in a Human Osteoarthritic Micro-Cartilage Model. *J. Cell Sci.* **2020**, *133* (23), jcs249094.

(33) Cannon, J. E.; Upton, P. D.; Smith, J. C.; Morrell, N. W. Intersegmental Vessel Formation in Zebrafish: Requirement for VEGF but Not BMP Signalling Revealed by Selective and Non-Selective BMP Antagonists. *Br. J. Pharmacol.* **2010**, *161* (1), 140−149.

(34) Boergermann, J. H.; Kopf, J.; Yu, P. B.; Knaus, P. Dorsomorphin and LDN-193189 Inhibit BMP-Mediated Smad, P38 and Akt Signalling in C2C12 Cells. *Int. J. Biochem. Cell Biol.* **2010**, *42* (11), 1802−1807.

(35) Daheshia, M.; Yao, J. Q. The Interleukin 1β Pathway in the Pathogenesis of Osteoarthritis. *J. Rheumatol.* **2008**, *35* (12), 2306−2312.

(36) Jenei-Lanzl, Z.; Meurer, A.; Zaucke, F. Interleukin-1β signaling in osteoarthritis − chondrocytes in focus. *Cell Signal* **2019**, *53*, 212−223.

(37) Valerio, M. S.; Edwards, J. B.; Dolan, C. P.; Motherwell, J. M.; Potter, B. K.; Dearth, C. L.; Goldman, S. M. Effect of Targeted Cytokine Inhibition on Progression of Post-Traumatic Osteoarthritis Following Intra-Articular Fracture. *Int. J. Mol. Sci.* **2023**, *24* (17), 13606.

(38) Allen, K. D.; Adams, S. B.; Mata, B. A.; Shamji, M. F.; Gouze, E.; Jing, L.; Nettles, D. L.; Latt, L. D.; Setton, L. A. Gait and Behavior in an IL1β-Mediated Model of Rat Knee Arthritis and Effects of an IL1 Antagonist. *J. Orthop. Res.* **2011**, *29* (5), 694−703.

(39) Elsaid, K. A.; Ubhe, A.; Shaman, Z.; D'Souza, G. Intra-Articular Interleukin-1 Receptor Antagonist (IL1-Ra) Microspheres for Posttraumatic Osteoarthritis: In Vitro Biological Activity and in Vivo Disease Modifying Effect. *J. Exp. Orthop.* **2016**, *3* (1), 18.

(40) Xia, P.; Wang, X.; Qu, Y.; Lin, Q.; Cheng, K.; Gao, M.; Ren, S.; Zhang, T.; Li, X. TGF-β1-induced chondrogenesis of bone marrow mesenchymal stem cells is promoted by low-intensity pulsed ultrasound through the integrin-mTOR signaling pathway. *Stem Cell Res. Ther.* **2017**, *8* (1), 281.

(41) Shen, H.; Lin, H.; Sun, A. X.; Song, S.; Wang, B.; Yang, Y.; Dai, J.; Tuan, R. S. Acceleration of Chondrogenic Differentiation of Human Mesenchymal Stem Cells by Sustained Growth Factor Release in 3D Graphene Oxide Incorporated Hydrogels. *Acta Biomater.* **2020**, *105*, 44−55.

(42) Hong, C.; Yu, P. Applications of Small Molecule BMP Inhibitors in Physiology and Disease. *Cytokine Growth Factor Rev.* **2009**, *20*, 409−418.

(43) Akash, M. S. H.; Rehman, K.; Chen, S. IL-1Ra and Its Delivery Strategies: Inserting the Association in Perspective. *Pharm. Res.* **2013**, *30* (11), 2951−2966.

(44) Rollins, B. J.; O'Connell, T. M.; Bennett, G.; Burton, L. E.; Stiles, C. D.; Rheinwald, J. G. Environment-Dependent Growth Inhibition of Human Epidermal Keratinocytes by Recombinant Human Transforming Growth Factor-Beta. *J. Cell. Physiol.* **1989**, *139* (3), 455−462.

(45) Acevedo Rua, L.; Mumme, M.; Manferdini, C.; Darwiche, S.; Khalil, A.; Hilpert, M.; Buchner, D. A.; Lisignoli, G.; Occhetta, P.; von Rechenberg, B.; Haug, M.; Schaefer, D. J.; Jakob, M.; Caplan, A.; Martin, I.; Barbero, A.; Pelttari, K. Engineered Nasal Cartilage for the Repair of Osteoarthritic Knee Cartilage Defects. *Sci. Transl. Med.* **2021**, *13* (609), No. eaaz4499.

(46) Majumder, N.; Mishra, A.; Ghosh, S. Effect of Varying Cell Densities on the Rheological Properties of the Bioink. *Bioprinting* **2022**, *28* (September), No. e00241.

(47) Sharma, A.; Desando, G.; Petretta, M.; Chawla, S.; Bartolotti, I.; Manferdini, C.; Paolella, F.; Gabusi, E.; Trucco, D.; Ghosh, S.; Lisignoli, G. Investigating the Role of Sustained Calcium Release in Silk-Gelatin-Based Three-Dimensional Bioprinted Constructs for Enhancing the Osteogenic Differentiation of Human Bone Marrow Derived Mesenchymal Stromal Cells. *ACS Biomater. Sci. Eng.* **2019**, *5* (3), 1518−1533.

(48) Gotoh, Y.; Tsukada, M.; Minoura, N. Chemical Modification of Silk Fibroin with Cyanuric Chloride-Activated Poly(Ethylene Glycol): Analyses of Reaction Site by Proton NMR Spectroscopy and Conformation of the Conjugates. *Bioconjugate Chem.* **1993**, *4* (6), 554−559.

(49) Dönges, L.; Schönenberger, M.; Bock, T.; Egloff, C.; Martin, I.; Barbero, A. A Developmental Biology Inspired Osteoarthritis 3din Vitromicro-Cartilage Model To Study Effects Of Pro-Anabolic And Anti-Inflammatory Factors On Tissue Homeostasis. *Osteoarthritis Cartilage* **2023**, *31*, S340−S341.

(50) Murab, S.; Chameettachal, S.; Bhattacharjee, M.; Das, S.; Kaplan, D. L.; Ghosh, S. Matrix-Embedded Cytokines to Simulate Osteoarthritis-like Cartilage Microenvironments. *Tissue Eng., Part A* **2013**, *19* (15−16), 1733−1753.

(51) Roy, S.; Sharma, A.; Ghosh, S. Macrophage Polarization Profiling on Native and Regenerated Silk Biomaterials. *ACS Biomater. Sci. Eng.* **2022**, *8* (2), 659−671.

(52) Srinivasan, A.; Rajendran, N. Surface Characteristics, Corrosion Resistance and MG63 Osteoblast-like Cells Attachment Behaviour of Nano SiO2-ZrO2 Coated 316L Stainless Steel. *RSC Adv.* **2015**, *5* (33), 26007−26016.

(53) Sharma, A.; Rawal, P.; Tripathi, D. M.; Alodiya, D.; Sarin, S. K.; Kaur, S.; Ghosh, S. Upgrading Hepatic Differentiation and Functions on 3D Printed Silk-Decellularized Liver Hybrid Scaffolds. *ACS Biomater. Sci. Eng.* **2021**, *7* (8), 3861−3873.

(54) Trucco, D.; Sharma, A.; Manferdini, C.; Gabusi, E.; Petretta, M.; Desando, G.; Ricotti, L.; Chakraborty, J.; Ghosh, S.; Lisignoli, G. Modeling and Fabrication of Silk Fibroin-Gelatin-Based Constructs Using Extrusion-Based Three-Dimensional Bioprinting. *ACS Biomater. Sci. Eng.* **2021**, *7* (7), 3306−3320.

(55) Bhattacharjee, M.; Chameettachal, S.; Pahwa, S.; Ray, A. R.; Ghosh, S. Strategies for Replicating Anatomical Cartilaginous Tissue Gradient in Engineered Intervertebral Disc. *ACS Appl. Mater. Interfaces* **2014**, *6* (1), 183−193.

(56) Admane, P.; Gupta, A. C.; Jois, P.; Roy, S.; Chandrasekharan Lakshmanan, C.; Kalsi, G.; Bandyopadhyay, B.; Ghosh, S. Direct 3D Bioprinted Full-Thickness Skin Constructs Recapitulate Regulatory Signaling Pathways and Physiology of Human Skin. *Bioprinting* **2019**, *15*, No. e00051.

(57) Roy, S.; Sharma, A.; Ghosh, S. Mechanistic Crosstalk of Extracellular Calcium-Mediated Regulation of Maturation and Plasticity in Human Monocytes. *Biochem. Biophys. Res. Commun.* **2023**, *643*, 39−47.

(58) Chakraborty, J.; Fernández-Pérez, J.; Van Kampen, K. A.; Roy, S.; Ten Brink, T.; Mota, C.; Ghosh, S.; Moroni, L. Development of a Biomimetic Arch-like 3D Bioprinted Construct for Cartilage Regeneration Using Gelatin Methacryloyl and Silk Fibroin-Gelatin Bioinks. *Biofabrication* **2023**, *15* (3), 035009.

(59) Das, S.; Pati, F.; Choi, Y. J.; Rijal, G.; Shim, J. H.; Kim, S. W.; Ray, A. R.; Cho, D. W.; Ghosh, S. Bioprintable, Cell-Laden Silk Fibroin-Gelatin Hydrogel Supporting Multilineage Differentiation of Stem Cells for Fabrication of Three-Dimensional Tissue Constructs. *Acta Biomater.* **2015**, *11* (1), 233−246.

(60) Wakefield, L. M.; Winokur, T. S.; Hollands, R. S.; Christopherson, K.; Levinson, A. D.; Sporn, M. B. Recombinant Latent Transforming Growth Factor Beta 1 Has a Longer Plasma Half-Life in Rats than Active Transforming Growth Factor Beta 1, and a Different Tissue Distribution. *J. Clin. Invest.* **1990**, *86* (6), 1976−1984.

(61) Ding, I.; Peterson, A. M. Half-Life Modeling of Basic Fibroblast Growth Factor Released from Growth Factor-Eluting Polyelectrolyte Multilayers. *Sci. Rep.* **2021**, *11* (1), 9808.

(62) Egan, G.; Phuagkhaopong, S.; Matthew, S. A. L.; Connolly, P.; Seib, F. P. Impact of Silk Hydrogel Secondary Structure on Hydrogel Formation, Silk Leaching and in Vitro Response. *Sci. Rep.* **2022**, *12* (1), 3729.

(63) Kang, F.; Yi, Q.; Gu, P.; Dong, Y.; Zhang, Z.; Zhang, L.; Bai, Y. Controlled Growth Factor Delivery System with Osteogenic-Angiogenic Coupling Effect for Bone Regeneration. *J. Orthop. Translat.* **2021**, *31*, 110−125.

(64) Kim, S. H.; Kim, S. H.; Jung, Y. TGF-β 3 encapsulated PLCL scaffold by a supercritical CO 2 −HFIP co-solvent system for cartilage tissue engineering. *J. Controlled Release* **2015**, *206*, 101−107.

(65) Xu, R.; Zhao, H.; Muhammad, H.; Dong, M.; Besenbacher, F.; Chen, M. Dual-Delivery of FGF-2/CTGF from Silk Fibroin/PLCL-PEO Coaxial Fibers Enhances MSC Proliferation and Fibrogenesis. *Sci. Rep.* **2017**, *7* (1), 8509.

(66) Chawla, S.; Midha, S.; Sharma, A.; Ghosh, S. Silk-based Bioinks for 3D Bioprinting. *Adv. Healthcare Mater.* **2018**, *7* (8), 1701204.

(67) Bell, D. M.; Leung, K. K.; Wheatley, S. C.; Ng, L. J.; Zhou, S.; Wing Ling, K.; Har Sham, M.; Koopman, P.; Tam, P. P.; Cheah, K. S. SOX9 directly regulates the type-ll collagen gene. *Nat. Genet.* **1997**, *16* (2), 174−178.

(68) Takahata, Y.; Hagino, H.; Kimura, A.; Urushizaki, M.; Yamamoto, S.; Wakamori, K.; Murakami, T.; Hata, K.; Nishimura, R. Regulatory Mechanisms of Prg4 and Gdf5 Expression in Articular Cartilage and Functions in Osteoarthritis. *Int. J. Mol. Sci.* **2022**, *23* (9), 4672.

(69) Zhong, L.; Huang, X.; Rodrigues, E. D.; Leijten, J. C. H.; Verrips, T.; El Khattabi, M.; Karperien, M.; Post, J. N. Endogenous DKK1 and FRZB Regulate Chondrogenesis and Hypertrophy in Three-Dimensional Cultures of Human Chondrocytes and Human Mesenchymal Stem Cells. *Stem Cell. Dev.* **2016**, *25* (23), 1808−1817.

(70) Franco, R. A. G.; McKenna, E.; Robey, P. G.; Shajib, M. S.; Crawford, R. W.; Doran, M. R.; Futrega, K. Inhibition of BMP Signaling with LDN 193189 Can Influence Bone Marrow Stromal Cell Fate but Does Not Prevent Hypertrophy during Chondrogenesis. *Stem Cell Rep.* **2022**, *17* (3), 616−632.

(71) Thielen, N. G. M.; van der Kraan, P. M.; van Caam, A. P. TGFβ/BMP Signaling Pathway in Cartilage Homeostasis. *Cells* **2019**, *8* (9), 969.

(72) Guo, X.; Wang, X. F. Signaling cross-talk between TGF-β/BMP and other pathways. *Cell Res.* **2009**, *19* (1), 71−88.

(73) Park, Y.; Sugimoto, M.; Watrin, A.; Chiquet, M.; Hunziker, E. B. BMP-2 Induces the Expression of Chondrocyte-Specific Genes in Bovine Synovium-Derived Progenitor Cells Cultured in Three-Dimensional Alginate Hydrogel. *Osteoarthritis Cartilage* **2005**, *13* (6), 527−536.

(74) Mehlhorn, A. T.; Niemeyer, P.; Kaschte, K.; Muller, L.; Finkenzeller, G.; Hartl, D.; Sudkamp, N. P.; Schmal, H. Differential effects of BMP-2 and TGF-β1 on chondrogenic differentiation of adipose derived stem cells. *Cell Prolif.* **2007**, *40* (6), 809−823.

(75) Chakraborty, J.; Mu, X.; Pramanick, A.; Kaplan, D. L.; Ghosh, S. Recent Advances in Bioprinting Using Silk Protein-Based Bioinks. *Biomaterials* **2022**, *287*, 121672.